NAVAL POSTGRADUATE SCHOOL

MONTEREY, CALIFORNIA

THESIS

EVALUATING THE FEASIBILITY OF 5G ENABLED DATALINKS FOR AVIATION COMMAND AND CONTROL

by

Brian J. White

June 2021

Thesis Advisor: John D. Roth
Second Reader: Raymond R. Buettner Jr.

THIS PAGE INTENTIONALLY LEFT BLANK

REPORT DOCUMENTATION PAGE			*Form Approved OMB No. 0704-0188*

1. AGENCY USE ONLY *(Leave blank)*	**2. REPORT DATE** June 2021	**3. REPORT TYPE AND DATES COVERED** Master's thesis

4. TITLE AND SUBTITLE EVALUATING THE FEASIBILITY OF 5G ENABLED DATALINKS FOR AVIATION COMMAND AND CONTROL	**5. FUNDING NUMBERS**
6. AUTHOR(S) Brian J. White	
7. PERFORMING ORGANIZATION NAME(S) AND ADDRESS(ES) Naval Postgraduate School Monterey, CA 93943-5000	**8. PERFORMING ORGANIZATION REPORT NUMBER**
9. SPONSORING / MONITORING AGENCY NAME(S) AND ADDRESS(ES) N/A	**10. SPONSORING / MONITORING AGENCY REPORT NUMBER**

11. SUPPLEMENTARY NOTES The views expressed in this thesis are those of the author and do not reflect the official policy or position of the Department of Defense or the U.S. Government.

12a. DISTRIBUTION / AVAILABILITY STATEMENT Approved for public release. Distribution is unlimited.	**12b. DISTRIBUTION CODE** A

13. ABSTRACT (maximum 200 words)

Per the 38th Commandant's Planning Guidance, the Marine Corps' forces must "operate and persist within range of adversary long-range fires." Marine command posts and units need to reduce their electromagnetic signatures to operate effectively in future conflicts. This constraint presents a particular challenge for aviation Command and Control (C2) operations because they rely on ultra-high frequency, omni-directional radio transmissions, which are highly susceptible to adversary direction finding systems. A possible solution to this problem is using low probability of detection millimeter wave (mmWave) communications enabled by the fifth generation (5G) cellular technology. Using 5G antenna array beam steering capability could create strong mmWave datalinks between aircraft and ground stations while the signal attenuates outside of the beam, remaining undetectable by an adversary. This research evaluated the feasibility of using 5G enabled mmWave communication for aviation C2 by observing the trade space between using narrow antenna beams and maintaining antenna pointing accuracy. The study found that given adequate signal-to-noise ratio, antenna pointing accuracy increased for arrays generating thinner beams at practical beamwidths when using signal direction of arrival estimation for antenna alignment. This finding indicates that mmWave communication system designs are not limited by beamwidth and have potential for aviation C2 applications.

14. SUBJECT TERMS 5G, fifth generation, Command and Control, C2, low probability of detection, signature management, aviation, millimeter wave, mmWave	**15. NUMBER OF PAGES** 81
	16. PRICE CODE

17. SECURITY CLASSIFICATION OF REPORT	**18. SECURITY CLASSIFICATION OF THIS PAGE**	**19. SECURITY CLASSIFICATION OF ABSTRACT**	**20. LIMITATION OF ABSTRACT**
Unclassified	Unclassified	Unclassified	UU

NSN 7540-01-280-5500 Standard Form 298 (Rev. 2-89) Prescribed by ANSI Std. 239-18

THIS PAGE INTENTIONALLY LEFT BLANK

Approved for public release. Distribution is unlimited.

EVALUATING THE FEASIBILITY OF 5G ENABLED DATALINKS FOR AVIATION COMMAND AND CONTROL

Brian J. White
Captain, United States Marine Corps
BS, United States Naval Academy, 2015

Submitted in partial fulfillment of the
requirements for the degree of

MASTER OF SCIENCE IN INFORMATION WARFARE SYSTEMS ENGINEERING

from the

NAVAL POSTGRADUATE SCHOOL
June 2021

Approved by: John D. Roth
Advisor

Raymond R. Buettner Jr.
Second Reader

Alex Bordetsky
Chair, Department of Information Sciences

THIS PAGE INTENTIONALLY LEFT BLANK

ABSTRACT

Per the 38th Commandant's Planning Guidance, the Marine Corps' forces must "operate and persist within range of adversary long-range fires." Marine command posts and units need to reduce their electromagnetic signatures to operate effectively in future conflicts. This constraint presents a particular challenge for aviation Command and Control (C2) operations because they rely on ultra-high frequency, omni-directional radio transmissions, which are highly susceptible to adversary direction finding systems. A possible solution to this problem is using low probability of detection millimeter wave (mmWave) communications enabled by the fifth generation (5G) cellular technology. Using 5G antenna array beam steering capability could create strong mmWave datalinks between aircraft and ground stations while the signal attenuates outside of the beam, remaining undetectable by an adversary. This research evaluated the feasibility of using 5G enabled mmWave communication for aviation C2 by observing the trade space between using narrow antenna beams and maintaining antenna pointing accuracy. The study found that given adequate signal-to-noise ratio, antenna pointing accuracy increased for arrays generating thinner beams at practical beamwidths when using signal direction of arrival estimation for antenna alignment. This finding indicates that mmWave communication system designs are not limited by beamwidth and have potential for aviation C2 applications.

THIS PAGE INTENTIONALLY LEFT BLANK

TABLE OF CONTENTS

LIST OF FIGURES

LIST OF TABLES

THIS PAGE INTENTIONALLY LEFT BLANK

LIST OF ACRONYMS AND ABBREVIATIONS

5G	Fifth Generation of Mobile Communication
AF	Array Factor
AOA	Angle of Arrival
BCT	Brigade Combat Team
C2	Command and Control
CAS	Close Air Support
DA2GC	Direct Air-to-Ground Communications
DARPA	Defense Advanced Research Projects Agency
DF	Direction Finding
DOA	Direction of Arrival
DOD	Department of Defense
EABO	Expeditionary Advanced Base Operations
EMCON	Emissions Control
EMS	Electromagnetic Spectrum
IoT	Internet of Things
LOS	Line-of-Site
LPI	Low Probability of Intercept
LPD	Low Probability of Detection
MACCS	Marine Air Command and Control System
MAGTF	Marine Air-Ground Task Force
mmWave	Millimeter Wave
PAT	Pointing, Acquisition, and Tracking
REC	Radio Electronic Combat
SNR	Signal-to-Noise Ratio
UAS	Unmanned Aerial System
UAV	Unmanned Aerial Vehicle
UHF	Ultra-High Frequency
ULA	Uniform Linear Array Antenna
USMC	United States Marine Corps

THIS PAGE INTENTIONALLY LEFT BLANK

ACKNOWLEDGMENTS

First, I would like to thank my thesis advisory team. Thank you, Professor Roth, for your guidance and helping me to organize my sometimes jumbled thoughts. Thank you, Dr. Buettner, for the initial introduction to 5G concepts. I would also like to thank Professor Smith for providing his instruction and helping to demystify telecommunications principles.

I am appreciative of the help that I received from all of the Naval Postgraduate School faculty and staff as well as my classmates during this journey. Finally, I am grateful for the thoughts and prayers from family and friends that supported me in ways that I may never know.

THIS PAGE INTENTIONALLY LEFT BLANK

I. INTRODUCTION

A. BACKGROUND

A key component of the United Sates Marine Corps (USMC) warfighting concept is combined arms integration, which involves coordinating air and surface delivered fires with ground forces maneuvers to overwhelm the enemy. The Marine Aviation Combat Element has achieved the coordination necessary for aviation fires through a robust command and control structure provided by the Marine Air Command and Control System (MACCS) and by integrating Forward Air Controllers and Joint Tactical Air Controllers with ground forces. Both the MACCS agencies and forward controllers have substantial communications capabilities to control aircraft employment and coordinate with each other. However, this communications capability may serve as a critical vulnerability in future conflicts because of its associated electromagnetic signature. With the advancements in direction finding (DF) capabilities and long-range precision fires, future adversaries will pose a significant threat to aviation command and control (C2) units.

The millimeter wave (mmWave) spectrum includes frequencies between 30 GHz and 300 GHz that were not previously used for typical wireless communication. The fifth generation of mobile communication technology (5G) will utilize mmWaves to provide users with higher bandwidth and faster data rates. One of mmWaves' characteristics is that they suffer from high link-loss over distances. However, using 5G antenna arrays' beamforming capability could potentially create a strong datalink between an aircraft and a ground station, while the signal attenuates outside of the beam remaining undetectable by an adversary. 5G technology could enable methods for low probability of detection (LPD) ground to air communications. This capability would allow aviation C2 units to better support Marines in future conflicts, including executing Expeditionary Advanced Based Operations (EABO).

B. PROBLEM STATEMENT

As the USMC shifts its focus to fighting against peer adversaries, there has been a larger emphasis on units better managing and minimizing their electromagnetic signatures.

This emphasis comes from the threat of enemy capabilities to use DF sensors to target friendly forces with long range fires. Electromagnetic signature management (SIGMAN) is particularly challenging for aviation C2 operations because they aim to produce a strong signal that is easily acquired by an aircraft's receiver. Consequently, aviation C2 units cannot practically employ many of the current signature management techniques. Using current communications equipment, it is not viable to provide adequate aviation C2 while lowering electromagnetic signature to desired levels.

C. PURPOSE STATEMENT

This research aims to test the feasibility for developing mmWave technology to provide a technical solution for electromagnetic signature management. Many current signature management practices are impractical for aviation C2 operations or would require a major shift in how Marines coordinate with aircraft and integrate air delivered fires. Providing Marine ground air controllers with LPD communication capabilities would allow the USMC to maintain its methods for controlling aircraft and mitigate enemy DF threats. Additionally, 5G and mmWave technology present an opportunity for improving communications throughout the USMC and across the Department of Defense (DOD). Millimeter wave communications provided higher data rates and enable more users. These attributes could be useful in controlling and collecting data from the increasing number of manned and unmanned systems in future operations. Finally, beamforming can apply to more than ground-to-air communications, so the research results may apply to surface-to-surface communications.

D. RESEARCH QUESTIONS

Primary question: What is the trade space between beamwidth and the received signal power, when tacking an aircraft to maintain proper antenna alignment?

Creating a more concentrated beam will provide higher antenna gain, delivering a better signal and lowering the probability of detection. However, the tighter the beam, the more difficult it will be to keep the aircraft within the antenna beamwidth.

Secondary question: Is there an optimal beamwidth for communications, based on this trade-off?

E. RESEARCH METHODS

This research created a model that simulated aircraft moving relative to a ground station and captured how difficult it is to keep each aircraft within a mmWave array antenna beamwidth. The Monte Carlo style simulation assessed a system's ability to estimate an aircraft position and transmit a beamformed mmWave signal towards that aircraft, using an array antenna. Also, aircraft movement and environmental parameters are varied to explore how they affect communications performance. This model evaluated the frequency and level of antenna pointing errors, which helped develop an understanding to the effort required to maintain beam alignment.

F. POTENTIAL BENEFITS, LIMITATIONS, AND RECOMMENDATIONS

This research provides an increased understanding of the potential benefits and requirements for applying 5G mmWave technology to aviation C2 applications. The outcome of the simulation also reveals the critical characteristics for a mmWave communications system. The primary limitation of this research is that it is a general study and does not observe the performance of an existing equipment. Also, assumptions made for simulation construction limit the scope of the research to a ground-to-air uplink. The research conclusion provides engineering recommendations and discusses if mmWave communications can meet aviation C2 operational requirements.

G. CHAPTER OUTLINE

Chapter II reviews current literature related to SIGMAN, 5G, and mmWave aviation communications. Chapter III describes the method for conducting the experiment and covers simulation design. Following, Chapter IV provides analysis of the simulation results. Chapter V concludes this research with assessment of the feasibility for using mmWaves for aviation C2 and recommendations for further research.

THIS PAGE INTENTIONALLY LEFT BLANK

II. LITERATURE REVIEW

A. COMMAND AND CONTROL NODE REQUIREMENTS

General David Berger's 38th Commandant's Planning guidance indicates that future C2 systems must maintain current communications capabilities, while reducing the associated electronic signature. Regarding C2 capabilities, General Berger states that "[w]e must create systems that are resilient and match our warfighting approach in order to protect our ability to make decisions that generate tempo" (Berger, 2019, p. 9). The Marine Corps warfighting approach is based on the maneuver warfare concept, which aims to rapidly exploit opportunities to gain battlefield advantages and defeat the enemy. Along with the need to make quick decisions, the Marine Air-Ground Task Force (MAGTF) relies communication and coordination between maneuver forces and fire support agencies to achieve the maximum combined arms effect on the enemy. The ability to effectively communicate is critical to tactical and operation success. Additionally, the future force will have to "operate and persist within range of adversary long-range fires" to effectively conduct the envisioned EABO concept (Berger, 2019, p. 12). EABO is an operational strategy that employs stand-in forces that work to disrupt enemy force, while operating within their engagement range. These stand-in forces will have to maintain a small signature, both physical and electronic, to avoid detection and targeting from adversaries. This requirement presents a challenge for C2 nodes because they typically have a large electromagnetic signature that is susceptible to DF. Furthermore, proposed support to forces executing EABO include High-Mobility Artillery Rocket System, unmanned systems, and loitering sensors and munitions (Berger, 2019). Employing these systems in the same airspace will involve significant coordination and integration. Even if future unmanned systems operate autonomously, they will need to occasionally reach back by a datalink or network to their supported unit. The requirements placed on future stand-in forces imply that their future C2 systems must operate in a way that counters future adversaries' emerging tactics and technologies.

B. COMMAND AND CONTROL NODE VULNERABILITIES

Future adversaries will look to use the electromagnetic spectrum (EMS) to disrupt Marine C2 systems with concepts like radio electronic combat (REC), which "is the integration of signals intelligence, target acquisition, and electronic attack/protection" practiced by the North Korea People's Army, the Chinese People's Liberation, and Russian Federation (Tsirlis, 2020, p. 77). REC aims to eliminate MAGTF capabilities that rely on communication or the EMS, such as headquarters, firing agencies, and units that support aviation operations. Because these units typically have a larger electronic signature, "[s]imple direction finding can precisely provide the location of friendly forces, which can easily provide targeting information for adversaries" (Tsirlis, 2020, p. 77). The increasing number of battlefield sensors, which can be prompted by this information to confirm or improve targeting data, amplifies this threat. This issue was displayed during the 2014 Battle of Zelenopillya between Russian and Ukrainian forces. After observing how the Russian's sensor-to-shooter capabilities allowed them to rapidly direct rocket artillery on Ukrainian units, the United States Army began reevaluating its brigade combat team (BCT) command posts (Greenberg, 2020). Like many organizations, BCT command posts have grown larger to support more data systems giving the commander increased intelligence and information sharing capabilities. However, with the growing threat against headquarters elements the Army is seeking to develop smaller signature, more mobile command posts to avoid engagement from long range, precision fires. Similarly, MAGTF planners have recognized that C2 elements will have to mitigate their electronic signatures to successfully operate in future conflicts.

Marine communications planners have focused their efforts to respond to this emerging threat by developing and practicing various electronic SIGMAN techniques. SIGMAN is deliberate action to remain hidden from the enemy to improve force protection and enable maneuver throughout the battlespace. Managing unit signatures directly impacts adversary intelligence capabilities, which supports conducting feints and forms of deception. SIGMAN procedures include remoting antennas, using directional antennas, terrain masking, adjusting maneuver to shield emissions, emissions control (EMCON), communications windows, brevity codes, setting radios on the lowest power setting, and

commander's intent and mission type orders (George, 2019). Combining these methods can reduce the MAGTF's electronic signatures, while allowing units to maneuver and coordinate surface fires. However, some of these techniques are impractical for aviation command and control operations. A large EMS is a noted limitation for MACCS agencies because aviation communications are typically reliant on ultra-high frequency (UHF) omnidirectional antennas. This issue also effects terminal air controllers that direct close air support (CAS) engagements.

UHF omnidirectional waveforms are used for ground to air communications because the directionless wave can reach aircraft traveling to and from various locations. This also enables ground forces to quickly establish ground to air communications and communicate on the move. Additionally, this waveform requires line-of-site (LOS), so MACCS agencies have limited abilities to employ terrain masking techniques. Remoting antennas can allow aviation C2 nodes to mask themselves with terrain by placing the antennas in a location with LOS, while the radios and personnel remain hidden. This technique can increase survivability for personnel and the radios themselves, but limits unit mobility by creating long emplacement and displacement times that also put units at risk (Greenberg, 2020). EMCON procedures limit the amount and type of emissions during operational phases to allow MAGTF forces to close towards objectives undetected. Nevertheless, if the scheme of maneuver requires aviation support, the radio transmissions required for coordination may not align with EMCON restrictions. Because coordinating aviation fires requires communication from the ground controller, "once a unit is conducting CAS, the gig is up" (W. DuBois, personal communication, 2020). Conducting an air assault or directing assault support operations would require similar communication from UHF omnidirectional radios. Unlike the ground forces practicing strict EMCON, CAS and air delivered assault support require high levels of coordination and cannot rely on mission type orders. Furthermore, MACCS agencies may need to communicate with aircraft to deconflict their flight paths with surface fires during shaping operations, when other units may plan to maneuver in communications silence. Administrative and operational SIGMAN procedures have limited applicability and effectiveness for aviation ground controllers because ground-to-air communication equipment is designed to have a

large EMS to facilitate reaching dispersed aircraft. This issue suggests that there needs to be a technical solution to effectively reduce the electronic signature associated with aviation C2.

C. 5G

5G refers to new radio-access technology, as well as three associated use cases: enhanced mobile broadband, massive machine-type communication, and ultra-reliable and low-latency communication (Dahlman et al., 2018). The development and transition to 5G will allow end users to simultaneously use more devices while downloading and transferring more data, at faster speeds. For example, downloading a high-definition movie in less than a second, compared to the approximately ten minutes it would take using previous 4G networks (Nordum & Clark, 2017). 5G achieves these improvements in latency and data rate from utilizing higher frequencies, providing access to more bandwidth. The frequency ranges 5G uses are mmWave, around 30 to 300 GHz, and sub-6, which uses frequencies below 6 GHz (closer to current cellular networks). Each frequency range has its advantages and disadvantages. Implementing "[a] 5G mmWave ecosystem would require a significant infrastructure build, but could reap the benefits of data transferred at up to [twenty times] the speed of current 4G LTE networks" (Medin & Louie, 2019, p.8). Creating a mmWave infrastructure is expensive because it must be constructed to overcome the waveform's poor propagation properties. High frequency electromagnetic waves have small associated wavelengths. Millimeter waves are blocked or absorbed by most objects in their propagation paths because of their shorter wavelengths. Also, as seen in Figure 1, these high frequencies suffer from greater oxygen absorption, especially between 50 GHz and 70 GHz (Harvey et al., 2019).

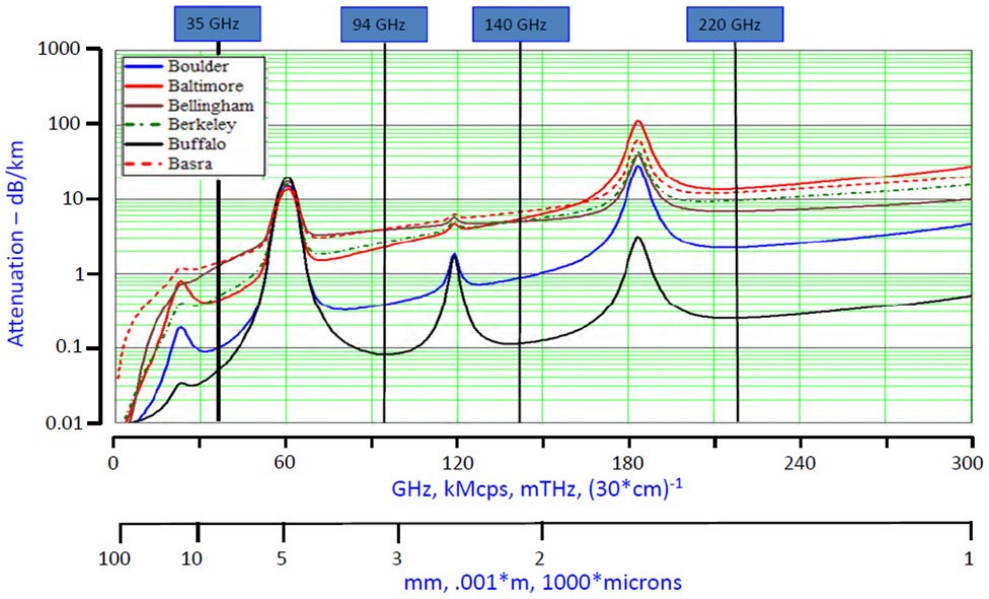

Figure 1. GHz Frequency Attenuation at Various Climates. Source: Wallace (2014).

This characteristic requires emplacing many base stations in an area to support network connectivity. However, mmWaves are necessary to achieve the maximum data rate and capacity increase provided by 5G technology. Also, mmWaves' propagation characteristics provide advantages from a physical layer security perspective. The rapid attenuation and absorption can prevent unintended listeners from receiving a signal. Additionally, smaller wavelengths result in smaller antennas "allowing for more compact deployment on wireless devices" (Medin & Louie, 2019, p. 8). In contrast, Sub-6 does not offer as significant increase in capabilities, but it is easier to implement because it does not suffer from mmWaves' propagation issues. Figure 2 displays the difference between mmWave and sub-6 signal propagation within a populated area.

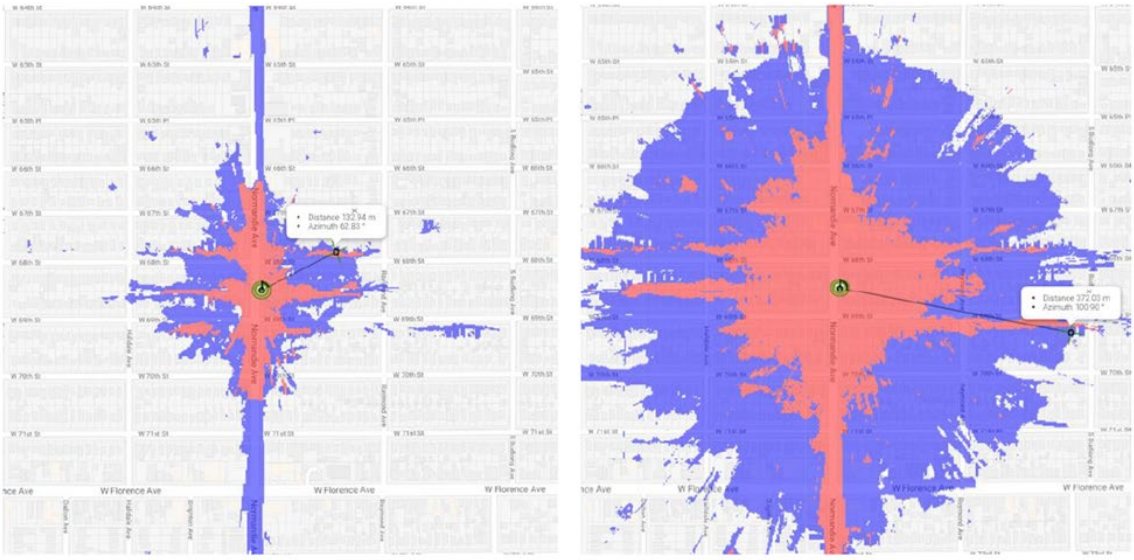

Figure 2. Difference in "Splat" Between mmWave (28 GHz) and sub-6 (3.4 GHz) Propagation. Source: Medin and Louie (2019).

As seen in Figure 2, sub-6 base stations provide considerably more coverage than their mmWave counterparts. This enables a sub-6 based network to have a lower upfront cost. However, the sub-6 waveform does not provide data-rate and latency improvements to the same extent as mmWaves because the sub-6 spectrum is already crowded. In summary, "[s]ub-6 is optimized for broad area coverage, which will make up a large part of the network, but mmWave may ultimately be able to provide more exquisite coverage in specific scenarios, and has some distinct military advantages in some topographies by virtue of being harder to intercept" (Medin & Louie, 2019, p. 11).

The difference between the initial investment needed to create a mmWave or sub-6 5G network has led to different approaches to 5G infrastructure development. Because sub-6 networks do not provide as significant of an increase in capabilities, the United States (US) has initially pursued a mmWave based architecture. Sub-6 based networks also create issues within the U.S. because the DOD reserves a substantial portion of that frequency band (Medin & Louie, 2019). Other countries, like China, have begun building a sub-6 based architecture because it is easier and has a lower upfront cost. Because sub-6 base stations provide wider area coverage, there are fewer base stations required to install for a

network. This reduced requirement combined with the ability to build from existing 4G infrastructure lowers the initial investment for sub-6 networks (Medin & Louie, 2019). As of 2020 China had deployed approximately 350,000 domestic 5G base stations, while their commercial manufactures (Huawei and ZTE) had shipped 10,000 base stations overseas (Medin & Louie, 2019). This is significant because sub-6 networks may become the international norm before mmWave based 5G. Although sub-6 frequencies do not provide inherent physical security like mmWaves, operating withing existing sub-6 architecture or with similar frequencies may make identifying specific military communications more difficult.

Two additional capabilities, associated with developing 5G array antenna technology, are massive multiple-input multiple-output (MIMO) and beamforming. Array antennas are singular antennas formed from numerous antenna elements, which can be used to alter and improve transmission and receiving characteristics. MIMO is a descriptor for a wireless system that can use multiple transmitters and receivers to communicate with separate devices simultaneously (Nordum & Clark, 2017). Massive MIMO improves upon previous capabilities to allow 5G base stations to support even more users and devices because the arrays have more antenna elements for use. This increased capacity will be beneficial in meeting future user demands from the growing Internet of things (IoT). Also, massive MIMO capabilities could potentially help support the need to communicate with the growing number of sensors and unmanned platforms employed by military units. A problem with implementing massive MIMO is that the increased antennas create challenges with more interference between channels, but 5G arrays' beamforming capability helps mitigate this issue. Beamforming empowers 5G base stations to use the spectrum more efficiently by sending data more directly to users, reducing interference between signals (Nordum & Clark, 2017). Additionally, beamforming helps overcome mmWave's propagation challenges by "focusing a signal in a concentrated beam that points only in the direction of a user, rather than broadcasting in many directions at once" (Nordum & Clark, 2017, Beamforming). This directed beam creates a higher antenna gain, overcoming mmWave's lossy characteristics and ensures a quality datalink between sender and receiver. Also, "[t]he narrower beam widths from antenna arrays, and the available

beam steering, offer lower probability of intercept (LPI) lower susceptibility to interference, and greater resistance to jamming and hacking (outside the beamwidth)" (Harvey et al., 2019, p. 52354). Beamforming improves mmWaves natural, physical security capabilities by further reducing signal spreading. With mmWave beamforming combined with its natural high attenuation, a signal would be difficult for an eavesdropper to detect outside of the beam. 5G technology introduces opportunities to support the continuously increasing systems on the battlefield, while potentially providing methods to mitigate electronic signatures.

D. 5G GROUND-TO-AIR COMMUNICATIONS

Because 5G promises more data transferred at faster rates, researchers are exploring how to 5G can support vehicular communications. These applications include ground vehicles, such as highspeed trains and self-driving cars, as well as manned and unmanned aircraft. Direct air-to-ground communications (DA2GC) is a concept that connects commercial aircraft to the ground cellular network to communicate with the crew and provide passengers with internet connectivity, shown in Figure 3.

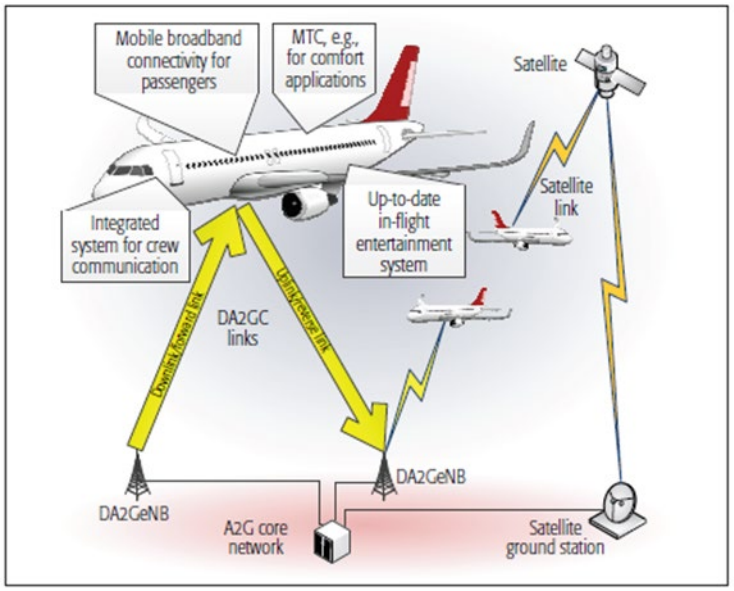

Figure 3. Visual Concept for DA2GC. Source: Vondra et al. (2017).

A study on transitioning from 4G to 5G for DA2CG using a 15 GHz frequency concludes that 5G is an excellent candidate because beamforming can provide a 17.5 dB signal-to-noise ratio (SNR), for 95% of the flight, while MIMO enables space division multiple access techniques providing each aircraft with a dedicated beam, preventing interference (Vondra et al., 2017). Another scaling study used a 3.7 GHz directional antenna to create a datalink between an unmanned aerial vehicle (UAV) finding that beamforming created a sufficient data rate; "[h]owever, one important thing to consider for beamforming is to track the aircraft so that the highest gain provided by the antenna is achieved for the DA2GC link" (Garcia et al., 2019 p. 314). Both studies modeled commercial aircraft communications, and they determined that utilizing 5G technology developments will meet their predicted needs for increased user data consumption. However, the limiting factor for achieving the desired data-rates is antenna beam alignment. An experiment addressing antenna beam tracking for 5G vehicular applications found "that a high data rate communication link can be reliably maintained during high angular speeds of the emulated vehicle by applying an appropriate, time and resource efficient tracking approach" (Heimann et al., 2019, p. 387). The results from this experiment suggest that applying knowledge about the expected situation of the transmitter and receivers will aid in maintaining connectivity. Considering a stationary base station and the vehicles anticipated movement will help mitigate beam alignment errors.

A demonstration of a bi-directional air-to-ground mmWave link confronted the antenna pointing challenge using a systems approach. The experiment used a E-band (71-86 GHz) link between a ground station and a Cessna aircraft flying at a 7 km altitude and top speed 463 km/h, and it achieved a sustained 40Gbps downlink and 36Gbps uplink (Tang et al., 2019). Although mmWave near this region can suffer from higher attenuation from oxygen, the study notes that with air-to-ground communication most atmospheric losses occur within the first few kilometer near the surface (Tang et al., 2019). The demonstration's communication system used a communications subsystem and a pointing, acquisition, and tracking (PAT) subsystem illustrated in Figure 4.

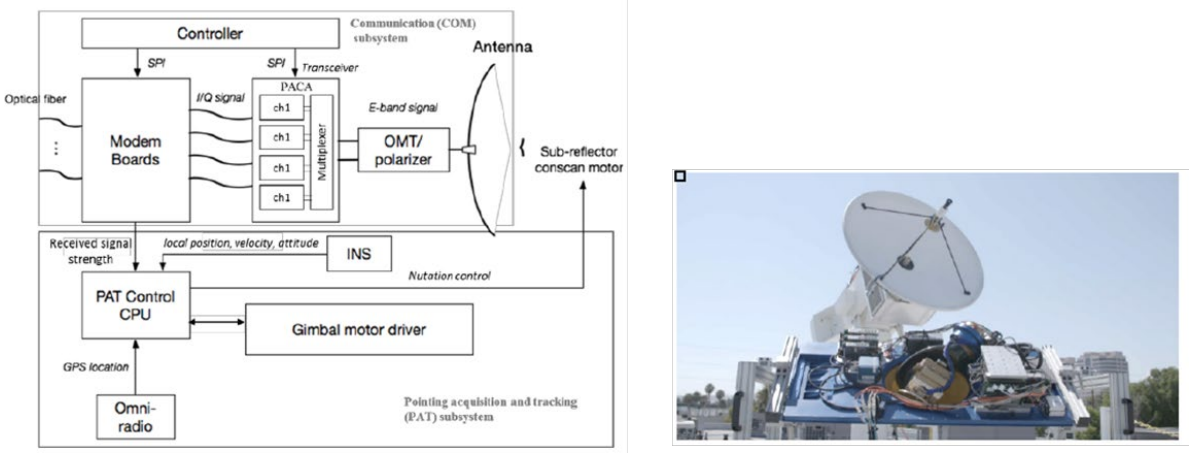

Figure 4. Communications System Block Diagram (Left) and Image of Communications System (Right). Source: Tang et al. (2019).

Responsible for maintaining a 0.05^{O} pointing accuracy, the PAT subsystem received position information from and inertial measurement unit and "and a low-data-rate but highly-sustainable discovery link, which is responsible for communicating initial position acquisition, data logging, management, and control" (Tang et al., 2019, p. 747). Sources of antenna pointing error were identified as stabilization errors and errors from the inertial navigation system position or calibration (Tang et al., 2019). This result further demonstrates the role of position information in successful mmWave communications. This experiments conditions parallel military CAS or assault support operations, demonstrating the potential for mmWave applications.

Similar to direct air-to-ground connections, mmWave ad hoc networks have demonstrated potential to provide connectivity to users. The Defense Advanced Research Projects Agency's (DARPA) Mobile Hotspots Program aimed to create to mesh network using mmWave frequencies to provide connectivity to mobile users on the ground. The system, employed by RQ-7 Shadow UAVs, used E-band frequencies with the goal of achieving gigabit data rates for the end user (Chandler, 2014, p. 26). Attaining this data-rate depended on PAT technologies and gimbaled mmWave radios to "support gigabit links via antenna gains of nominally 40 dB and corresponding beamwidth of ~2 degrees" (Chandler, 2014). The results from the Mobile Hotspots Program reinforce that mmWaves can enhance communications capabilities in mobile environment if there is adequate vehicle tracking.

In addition to providing increased capacity and data-rates, 5G mmWaves natural physical security characteristics make it an attractive technology for both civilian and military applications. Beamforming and MIMO can support many civilian IoT devices while limiting interference, and they can help military organizations employ more sensors and unmanned vehicles. An issue that effects both sectors is that "robotic vehicles have proven vulnerable to external manipulation, not only of their communications, but through the wireless link with an adversary directing control of their navigation and control systems" (Harvey et al. et al., 2019, p. 52353). This risk could be mitigated by mmWaves' inherent resistance to signal manipulation. The increased security capability could be useful for both direct links and communications relays. A study of the secrecy rate of UAV enabled mmWave relays showed that they were effective at transmitting information between two distributed sources while avoiding eavesdropper detection, shown in Figure 5. They defined the average secrecy rate as the difference between the average data rates from the source to the desired destination and to an eavesdropper (Sun et al., 2019). The study determined that with perfect beam alignment the fading gain for the legitimate communications link is greater than the eavesdropping link providing adequate secrecy rates, especially at higher frequencies (Sun et al., 2019).

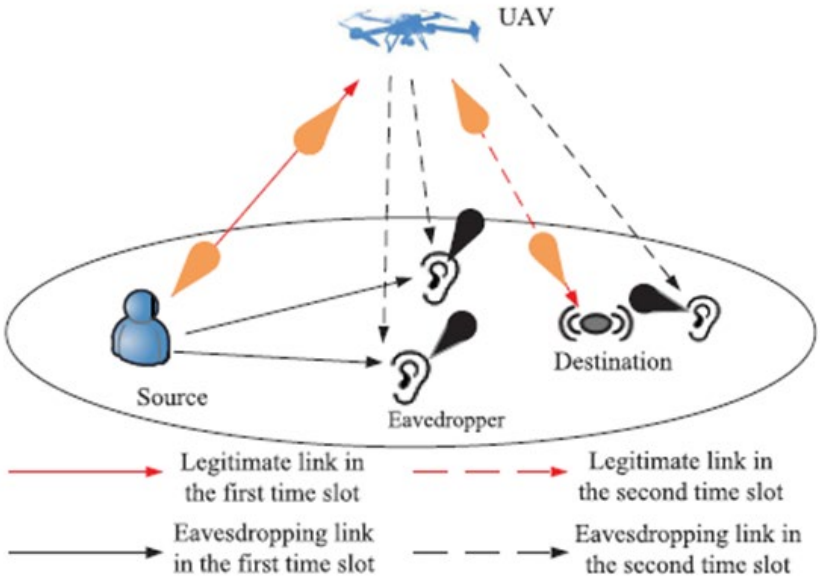

Figure 5. UAV Relay Physical Security Scenario. Source: Sun et al. (2019).

These results show how mmWaves could be useful for creating a covert, high-capacity link with an aircraft or extending the link into a network. Like the requirements to achieving the maximum data-rate, achieving the greatest security relies on proper antenna alignment. Steerable beams reduce the probability of the radio signals being detected or jammed, but advanced array antennas introduce system-level challenges with the information required for beam steering and calibration (Hosseini et al., 2019). Again, mmWave present the potential for transformative capabilities, but are limited by the need to maintain beam alignment. Also, to truly remain undetected a beam should be as narrow as practical, which would increase beam tracking difficulty. Using beamforming for aviation communications will depend on the ability to effectively steer the beams. Consequently, identifying how difficult it is to maintain acquisition of an aircraft will help determine if implanting 5G mmWave communications is feasible.

III. EXPERIMENT METHOD

This chapter will cover design for the experiment conducted with this research. The purpose of this experiment was to answer the primary research question by investigating beamwidth to acquisition tradeoff for mmWave communications datalinks. Also, the goal for this investigation was to present data for future engineering decisions, so the effects of the number of antenna elements, SNR, and aircraft speed were captured. This experiment was conducted with a simulation that is described in the following sections.

A. ASSUMPTIONS

Because the experiment evaluated aircraft tracking capabilities without an existing tracking method, assumptions had to be made to construct the simulation. First, a dead reckoning method for motion tracking was inappropriate for this application. The tracking method needs to support varying and dynamic flight paths, so the transmitting ground station could not assume a consistent starting and end point for an aircraft. For this reason, the experiment simulates that the aircraft initiates radio communication or uses a "ping" transmission that the ground station uses for geolocation. Furthermore, this assumption limits the experiment to focusing on a mmWave uplink. Examining the uplink is more important than the downlink because one of the major benefits from using mmWave communications would be better protecting the ground stations. Also, with eventual tracking techniques, it should be easier to maintain antenna alignment for the downlink because the ground station would not typically move during communication. Lastly, the experiment ignored aircraft elevation, and it was performed in two dimensions. This decision simplified the problem because there was limited value added when working in three dimensions. These assumptions allowed for simulation design and execution.

B. ARRAY ANTENNA THEORY

Many mmWave communications use array antennas because of their capabilities and flexibility. Antennas, known as phased arrays, have "the ability to shape the pattern through spacing and excitation adjustment along with the unique capability of scanning the pattern in angular space by dynamically adjusting the excitation phases electronically"

(Stutzman & Thiele, 2013, p.271). This capability is especially useful because it allows antenna arrays to operate without supporting mechanical components, to steer beams at electronic speeds, and to create multiple simultaneous beams (Stutzman & Thiele, 2013). When an array antenna is constructed from identical antenna elements, equally spaced along the same axis, it is known as a uniform linear array antenna (ULA). In Figure 6, r is a vector from an incoming plane wave. The space between elements, d, is often a half-wavelength because it causes one period of the beam pattern to appear in the visible region, whereas longer wavelengths would generate additional major lobes in the visible region (Stutzman & Thiele, 2013).

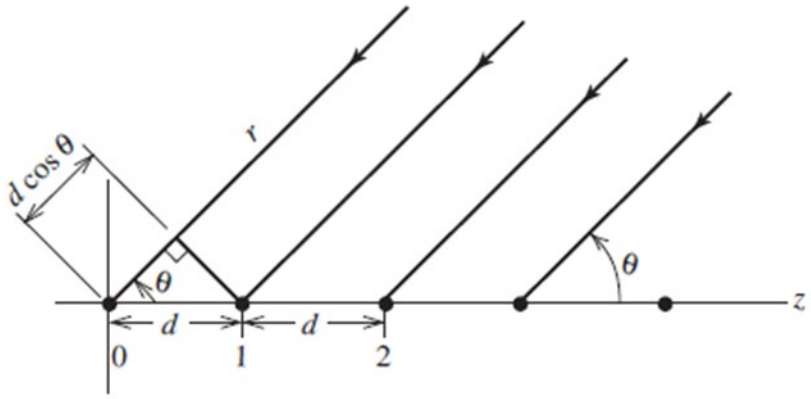

Figure 6. Linear Array of Equally Spaced Isotropic Point Sources. Source: Stutzman (2013).

These are known as grating lobes. Because an array antenna beam pattern is periodic, the visible region refers portion of the pattern that radiates into space (T. Smith, personal communication, 4 Feb 2021). The beam pattern, or array factor (AF) for a two-point source array is displayed in Figure 7.

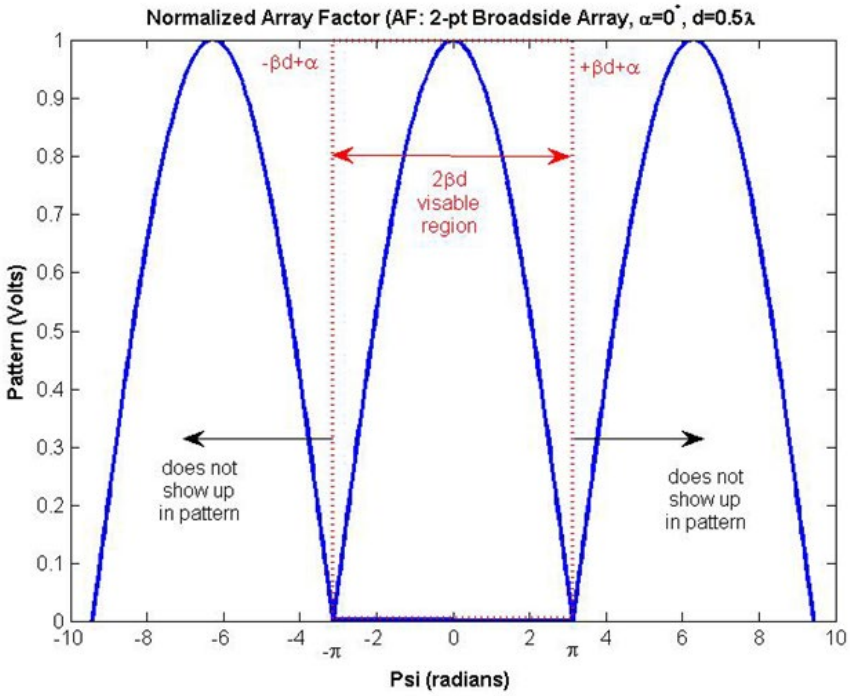

Source: T. Smith, personal communication, Feb 4, 2021.

Figure 7. Normalized Array Factor for Two-Point ULA

Figure 7 illustrates the two additional lobes are not visible because d is a half-wavelength. Also in Figure 6, β is the phase constant, and α is the element phase. When α is zero, the points are described as "in phase" and produce the maximum array pattern perpendicular, or broadside, to the array axis (T. Smith, personal communication, 4 Feb 2021). This concept is displayed in Figure 8. More information regarding the simulated ULAs used in the experiment and their applications will be discussed later in this chapter.

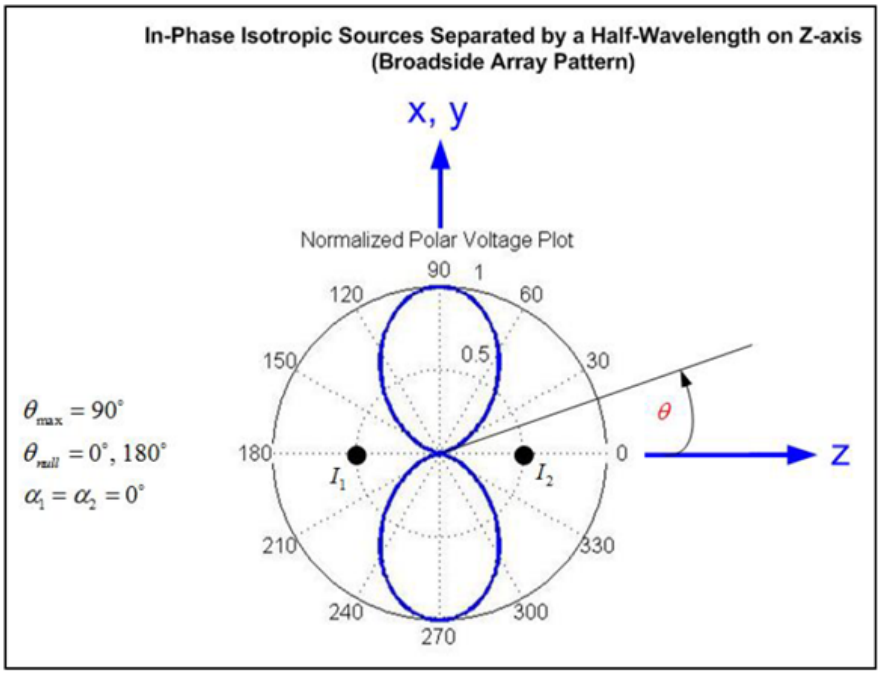

Source: T. Smith, personal communication, Feb 4, 2021.

Figure 8. Broadside Array Pattern for Two-Point ULA

C. DIRECTION FINDING THEORY

DF is the process of collecting incoming electromagnetic waves and using their characteristics to determine the direction of the source. The basic methods for direction finding rely on measuring the fundamental properties of electromagnetic waves, which are the direction of magnetic field vectors (polarization) or the orientation of surfaces with equal phase (Rhode & Schwarz, 2011). Advances in array antenna and signal processing capabilities have built on previous DF techniques. DF using a sensor array can receive multiple incoming waves and determine their number, direction of incidence, and amplitude (Rhode & Schwarz, 2011). Figure 9 shows the basic DF scenario, and Figure 10 displays the architecture for DF with a sensor array.

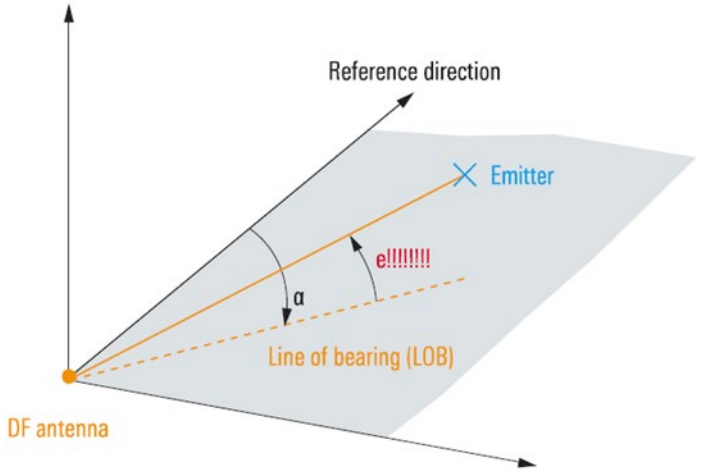

Figure 9. Figure 8. Basic Emitter Detection. Source: Rhode and Schwarz (2011).

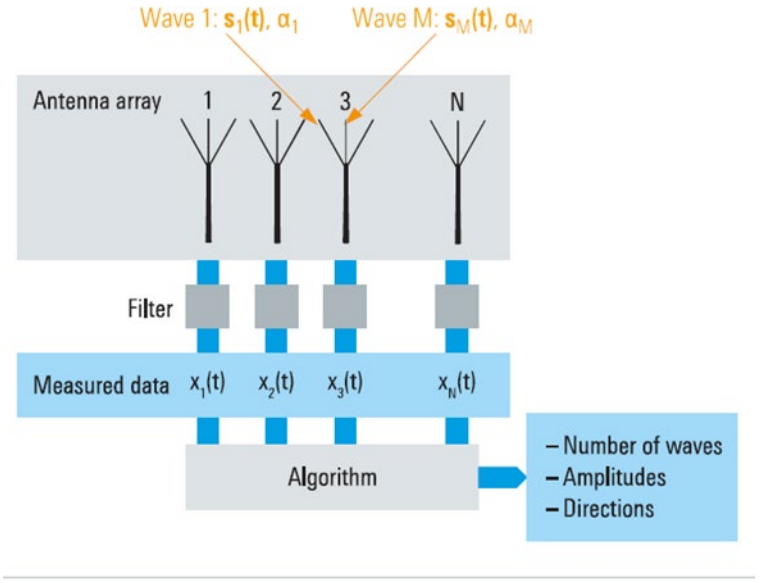

Figure 10. Basic DF Antenna Array Task. Source: Rhode and Schwarz (2011).

Antenna arrays can be used to perform subspace-based methods, of which the Multiple Signal Classification (MUSIC) algorithm has become an alternative to most direction of arrival (DOA) methods because it obtains arbitrary accuracy provided

sufficient SNR (Krim & Viberg, 1996). Subspace DF methods mitigate noise effects by splitting space into N-dimensions based on the array antenna outputs (Rhode & Schwarz, 2011). The MUSIC algorithm uses vectors to identify signals within these subspaces. Signal vectors are perpendicular to the noise subspace, so nulls in direction vectors that point into a subspace identify signals, which can be used for a DF function (Rhode & Schwarz, 2011). A limitation of the MUSIC algorithm is that it fails to resolve closely space, correlated signals (Krim & Viberg, 1996). Also, the number of incoming signals must be known. MUSIC can be used for any antenna array geometry; however, ULAs can utilize Root-MUSIC, which is the polynomial rooting version of MUSIC and has shown superior performance (Krim & Viberg, 1996). The Root-MUSIC algorithm supports the DF functions in this simulation because it uses a ULA.

D. SIMULATION DESIGN

The simulation assesses how the beamwidth, aircraft speed, and ground station DOA estimator's SNR affect the ground station's ability to track a moving aircraft. The simulation was constructed in MATLAB based on flowchart in Figure 10.

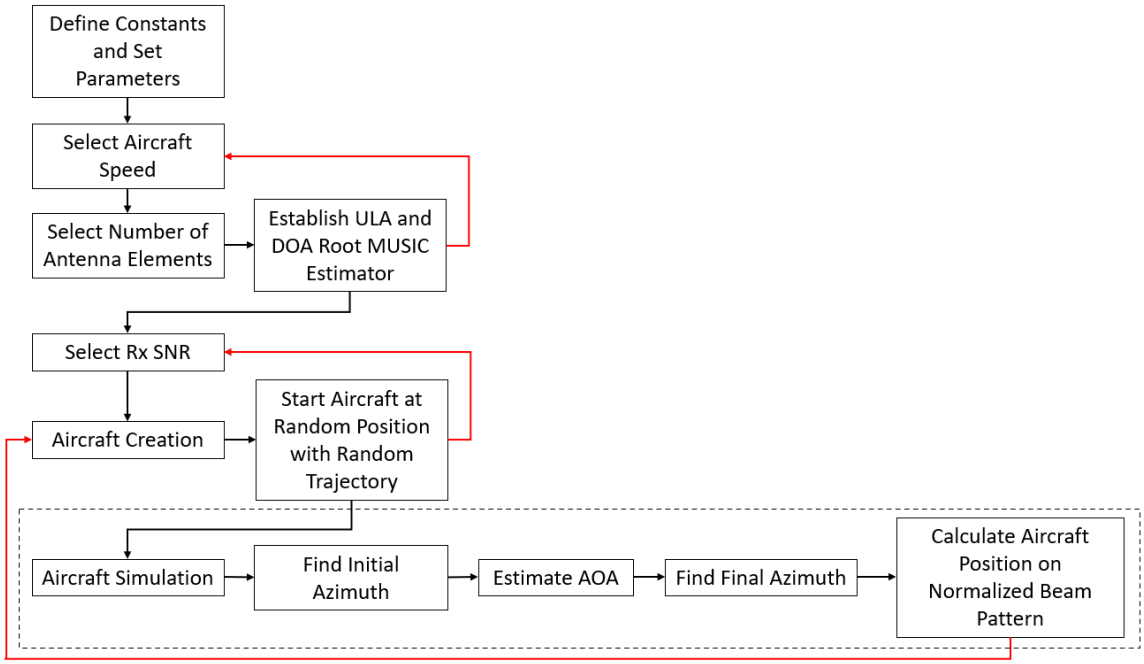

Figure 11. Simulation Construction Flowchart

The simulation was built using a series of nested "for" loops. The black arrows represent the forward progression of the model. The red arrows show the points at which each loop finishes and returns to the previous loop, for the next iteration. The final section, surrounded by the dashed line, signifies the "for" loop needed to simulate the aircraft motion and conduct calculations. The complete MATLAB code is in Appendix A.

Defining constants, setting parameters, and making initial calculations established the experiment space. The transmitter used a 30 GHz transmitter carrier frequency because it is at the lower end of the mmWave spectrum and would have favorable propagation characteristics. Also, the transmitter used the ideal half-wavelength spacing between each antenna element. Simulated aircraft generated within a 50km-by-50km square with the ground station at the center. A 50km distance was chosen because it is the approximate length of Okinawa, Japan, so this size represents a notional expeditionary advanced base. Table 1 contains the aircraft speeds and number of antenna elements (N), with associated lengths and half-power beamwidths (HPBW), used for the simulation.

Table 1. Simulation Parameters

Speed (m/s)	N	Length (m)	HPBW (deg)
0.25	2	0.01	52.5909
38	24	0.1199	4.2313
75.75	46	0.2298	2.2073
113	68	0.3398	1.4931
151.25	90	0.4497	1.1281
189	112	0.5596	0.9065
226.75	134	0.6695	0.7577
264.5	156	0.7795	0.6508
302.5	178	0.8894	0.5704
340	200	0.9993	0.5076

In addition to the parameters above, the ground station's received SNR was varied from -10dB to 20dB in increments of 5dB. The low end of the speed represents a small unmanned aerial system (UAS), while the highest speed is approximately Mach One to

capture how speed would affect antenna pointing for various types of aircraft. The number of antenna elements, N, went from the minimum amount to an array length of approximately one meter to explore how size constraints would affect performance. The HPBW was calculated using the following equation, where d is the antenna element spacing (T. Smith, personal communication, 25 Feb 2021).

$$HPBW = 2\arcsin\left(\frac{0.443\lambda}{Nd}\right) \tag{1}$$

Following the constants and parameter definitions, the simulation selected a configuration from ten speeds, ten array lengths, and seven SNRs. Each trial generated one thousand aircraft, collecting ten data points per aircraft, for a total of seven million data points. A sample was taken every six seconds to represent a minute of communications. The first parameter selected was speed, with no direct follow-on action. Following the speed selection, the simulation chose the number of antenna elements and created the ULA for the ground station. The ULA was created using the MATLAB Phased Array System Toolbox. The toolbox's ULA object creates a ULA based given properties (MathWorks, phased.ULA). This simulation input the number of elements, N from the previous table, and antenna spacing of 0.005 m, the associated half-wavelength to the 30 GHz transmit frequency, into the ULA object. The antenna kept the default settings of isotropic elements, no element tapering, and antenna alignment along the Y axis.

Utilizing this ULA as an input, the Phased Array System Toolbox Root MUSIC Estimator object simulated the ground station's DOA capability. The estimator object required indication of the number of incoming signals, which directly related to the stated limitation of the MUSIC algorithm. Because the experiment observed one aircraft at a time, the number of incoming signals was set to one. The simulation initially used the default 300 MHz operating frequency for the estimator received signal, which represented an omnidirectional, initial transmission or ping that the aircraft would send a ground station to use for antenna alignment. This decision assumed that the aircraft would not have position information for the ground station, so it would have to use a directionless signal to initiate communication. However, if an aircraft had position information for the

stationary ground station, it could direct its initial transmission to establish communication. This notion led to follow-on experimentation, which will be discussed in the following section. The MATLAB ULA object construction does not account for losses due to impedance mismatching caused by the difference between the actual and ideal antenna element size. The ideal antenna element size is a half-wavelength, so the initial experiment simulated a ULA with 0.5 m antenna elements to match the received 300 MHz frequency. An array designed for collection of the 300 MHz signal should also have 0.5 m element spacing. However, such large spacing would result in an especially long array when using many antenna elements, so the spacing remained at 5 mm. The observation of the initial experiment's simulated ULA is interesting because it balanced compactness with the ability to receive lower frequencies.

The next loop selects the SNR for the signal received by the DOA estimator, before continuing to the loops used for aircraft generation and communications simulation. Each aircraft was generated using the "model platform motion" object within the Phased Array System Toolbox (MathWorks, phased.Platform). This tool creates a platform that can then move within space at a constant velocity. The aircraft began in a random location within the theoretical airspace and moved in a random direction, at the selected speed. After creating an aircraft and assigning its trajectory, the simulation executes platform motion and evaluates communications performance, which is illustrated in Figure 12.

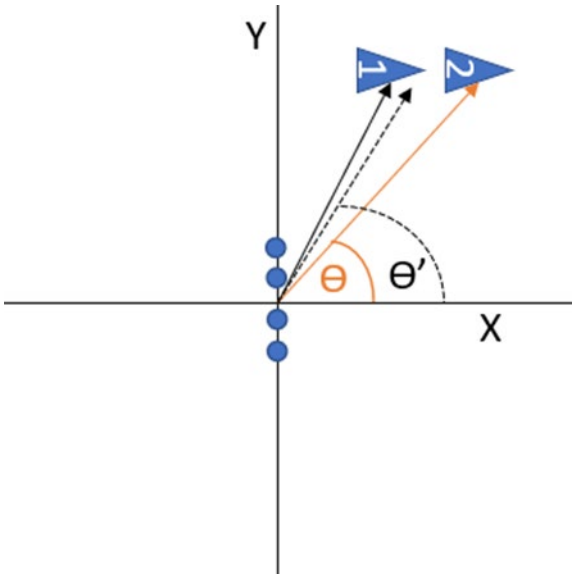

Figure 12. Simulation Illustration

Figure 12 depicts the function of the last loop within the experiment. The triangle labeled with "1" represents the aircraft as it sends its emission. The triangle labeled "2" is the aircraft after its displacement during the time it took for a two-way transmission with the ground controller. First, a plane wave is generated from position "1" for the DOA estimator to collect. The MATLAB Communications Toolbox has an additive white gaussian noise function, which applies noise to signal based on the corresponding SNR. This signal fed into the previously constructed DOA estimator, which returned an estimated angle of arrival (AOA). This estimated AOA is shown as the dotted arc or Θ' in Figure 12. The time for a two-way communication is calculated based on the speed of light and the distance from "1" to the ground controller, at the origin. The distance the aircraft traveled in this time is position "2," and its azimuth is displayed as the orange arc or Θ in Figure 12. Therefore, Θ identifies the aircraft's actual position, while Θ' indicates the estimated position. When combined, these angles reveal the antenna pointing error. This process repeats ten times, every six seconds to simulate one minute of communication.

For this simulation, the actual position of the aircraft within the transmitting antenna's beam pattern measures the performance of the mmWave communication system. Observing how far off of boresight the actual position is in the normalized beam pattern

essentially returns the percentage of signal power an aircraft's communication system would receive. The following function describes the normalized beampattern, or array factor (AF), for a ULA (Stutzman & Thiele, 2013).

$$f(\psi) = \frac{\sin\left(N\frac{\psi}{2}\right)}{N\sin\left(\frac{\psi}{2}\right)} \tag{2}$$

The phase difference between array elements, Ψ , drives the antenna beampattern function. It can be found with the following equations (Stutzman & Thiele, 2013).

$$\psi = \beta d\cos\theta + \alpha \tag{3}$$

where, β is the phase constant, and α is the element phase based on antenna pointing angel.

$$\beta = 2\pi/\lambda \tag{4}$$

$$\alpha = -\beta d\cos\theta_o \tag{5}$$

In the previous expressions, Θ represents the angle of the incoming wave, and Θ_o is the antenna main beam scanning angel. Together these equations express the phase difference between antennas when the ULA is directed off of boresight (Stutzman & Thiele, 2013).

$$\psi = \beta d\left(\cos\theta - \cos\theta_o\right) \tag{6}$$

Figure 13 provides an illustration of the situations described by the previous equations.

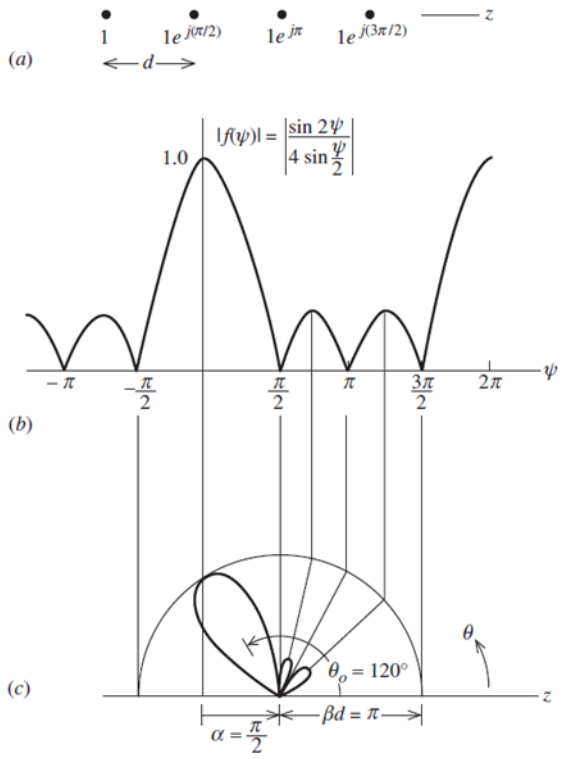

Figure 13. Four Element ULA Response with 120º Main Beam Scan Angle. Source: Stutzman (2013).

As seen in the Figure 13, the angles are measured from the array axis. However, in in this experiment, the angles are measured relative to the X axis, while the array is positioned along the Y axis. The requires replacing the cosine expressions with sine expressions, when calculating Ψ. Also, Θo from the Figure 13 and the previous equations is equivalent to Θ' from Figure 12. Finally, considering that the element spacing, d, is half of a wavelength, the expression for the phase difference between elements in the simulation is below.

$$\psi = \pi\left(\sin\theta - \sin\theta'\right) \tag{7}$$

This expression with the function for a ULA normalized beam pattern provides an equation to calculate where an aircraft lies in the transmitter beam (J. Roth, personal communication, 22 Apr 2021).

$$AF_{Normalized} = \frac{\sin\left(\frac{N\pi}{2}\left(\sin\theta - \sin\theta'\right)\right)}{N\sin\left(\frac{\pi}{2}\left(\sin\theta - \sin\theta'\right)\right)} \tag{8}$$

The normalized AF equation returns a value between zero and one, that characterizes the ratio of the transmitted power a target antenna would receive based on antenna pointing. This value was chosen as the measure of performance because of the numerous unknown variables in a communications scenario. Because communications systems have different performance levels and requirements, this metric can help engineers understand the limiting factors for mmWave communications. Additionally, a goal for this experiment was to investigate the computational effort required to maintain a mmWave data link. The normalized AF helps to convey that effort because it captures how often a target antenna would receive power below the necessary threshold for communication. This will aid engineers in evaluating how often their antenna beam steering equipment could have to sense the environment to maintain a target.

E. FOLLOW-ON EXPIRIMENTATION

As previously stated, the initial experiment investigated if a ground station could track an aircraft transmitting a directionless UHF signal; however, the follow-on experiment explored how the ground station would respond if the aircraft used a directed mmWave downlink. This simulation assumed that the aircraft could locate and direct a mmWave signal to a stationary ground controller. The follow-on experimentation consisted of two additional iterations of the simulation. These repetitions still observed the uplink only, but they represented a downlink with a mmWave carrier frequency, vice UHF, by increasing the operating frequency of the DOA estimator's received signal from 300 MHz to 30 GHz. Again, the ULA object did not account for losses due to the antenna size, so the antenna elements were simulated as 5 mm for this experiment. However, unlike the previous experiment, the increased downlink frequency corresponded to the antenna element spacing. In this simulation, both the antenna element length and the spacing were 5 mm, which matched the half-wavelength of the 30 GHz operating frequency. Also, this set of experimentation modified the simulation parameters based on the results from the initial experiment, which are covered in detail in Chapter IV. It used the same previously

covered MATLAB model, but this version did not vary speed and observed an increased SNR range. The follow-on simulation maintained aircraft speed at 65 m/s, which is the approximate transiting speed for a helicopter. Because of the importance of SNR on system performance, this model expands the SNR range to -20dB to 20dB. Finally, the follow-on simulation used arrays with a smaller number of elements to provide better understanding of performance for shorter arrays. Tables 2 and 3 show the array lengths, using half wavelength element spacing, and associated HPBWs for the follow-on and final simulations, respectively.

Table 2. Follow-On Simulation Parameters.

N	Length (m)	HPBW (deg)
2	0.01	52.5909
14	0.07	7.2569
26	0.129	3.9057
38	0.1899	2.672
50	0.2498	2.0307
62	0.3098	1.6376
74	0.3697	1.372
86	0.4297	1.1806
98	0.4897	1.036
110	0.5496	0.923

Table 3. Final Experiment Parameters.

N	Length (m)	HPBW (deg)
2	0.01	52.5909
8	0.04	12.7171
14	0.07	7.2569
20	0.0999	5.0781
26	0.1299	3.9057
32	0.1599	3.1732
38	0.1899	2.672
44	0.2198	2.3076
50	0.2498	2.0307
56	0.2798	1.8131

IV. RESULTS AND ANALYSIS

This chapter presents the results of the simulation discussed in Chapter III. Also, it covers follow-on experimentation inspired by the initial simulation results. Analysis of the results from each version of the experimentation explore how each parameter affected antenna pointing accuracy. This chapter's final section discusses the impact of the findings on designing communications systems.

A. SIMULATION OUTPUT

As stated in the previous chapter, the model simulated aircraft moving relative to a ground station in two dimensions. Figure 14 is a visual depiction of the simulation platforms.

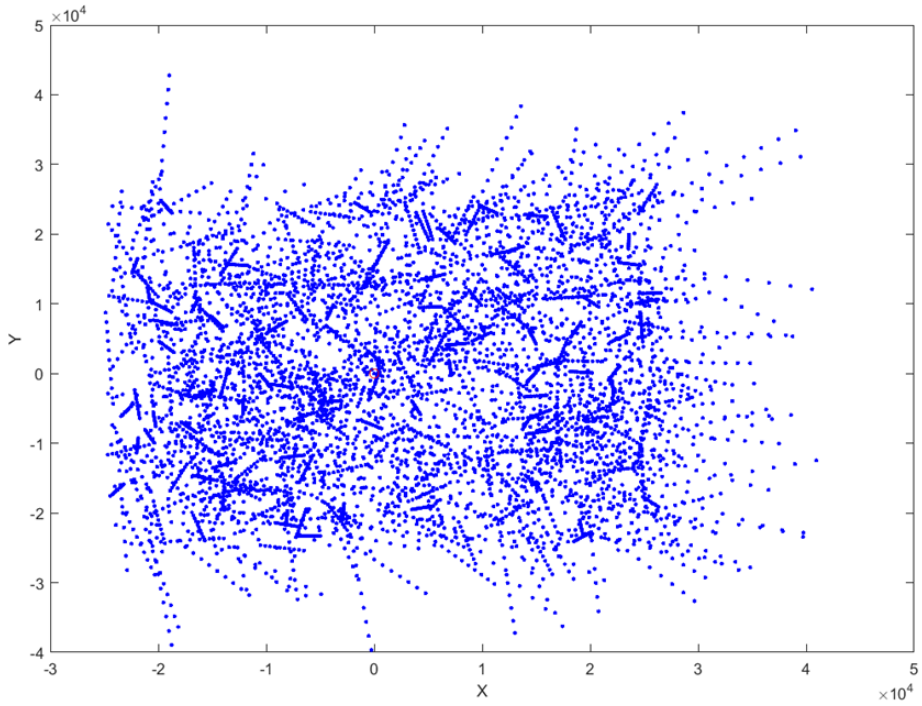

Figure 14. Graphic of Simulation Platforms

The red circle at the center of the plot represents the ground station. While the series of blue dots are the aircraft moving through space. As seen in Figure 14, the aircraft originate and move in various directions, and ten samples were collected for each trial. At

each point, the actual and estimated AOA were found to calculate the normalized AF. The model results were captured by storing each calculated AF into a series of matrices and cell arrays. This grouped the results, so they could be analyzed based on the varying parameters.

B. SIMULATION RESULTS

The primary tool for chosen for data analysis is the empirical cumulative distribution function (ECDF) because it provides a method to compare how different parameters affected performance during the Monte Carlo trials. The ECDF takes a set of data and depicts values on the X axis. It then computes the probability of an occurrence below the associated the X axis value and shows the probability on the Y axis. The data was reorganized based on the values of the speed, number of antenna elements (N), and SNR settings to assess each parameter's impact on AOA estimation. For example, the results from every trial with a N value of 24 were put into the same array. These data points include results from every combination of speed and SNR, but only for when N is 24. The ECDF calculation used this group of data to effectively isolate each aircraft speed, N, or SNR, when observing each property's effect on performance. This process was repeated for every value of every parameter. Then, plotting the ECDFs of the same kind together, on the same figure, displayed the overall relationship between that characteristic and performance. In the following ECDFs, the curves that remain flat along the X axis as they move to the right indicate better performance.

1. Speed

The experiment varied aircraft speed to see if it would affect antenna alignment, and to investigate if mmWave communications would be suitable for use with different types of aircraft. AOA estimation error is the initial source of antenna pointing inaccuracy. Likewise, aircraft speed could contribute to pointing error due to the aircraft's displacement, during the time it takes for the aircraft's initial transmission and the ground station's response to travel through space. The ECDFs for the results of varying speed are shown in Figure 15. The X axis shows the normalized AF, which represents a ratio of the maximum power provided based on the aircraft position within the antenna's beam.

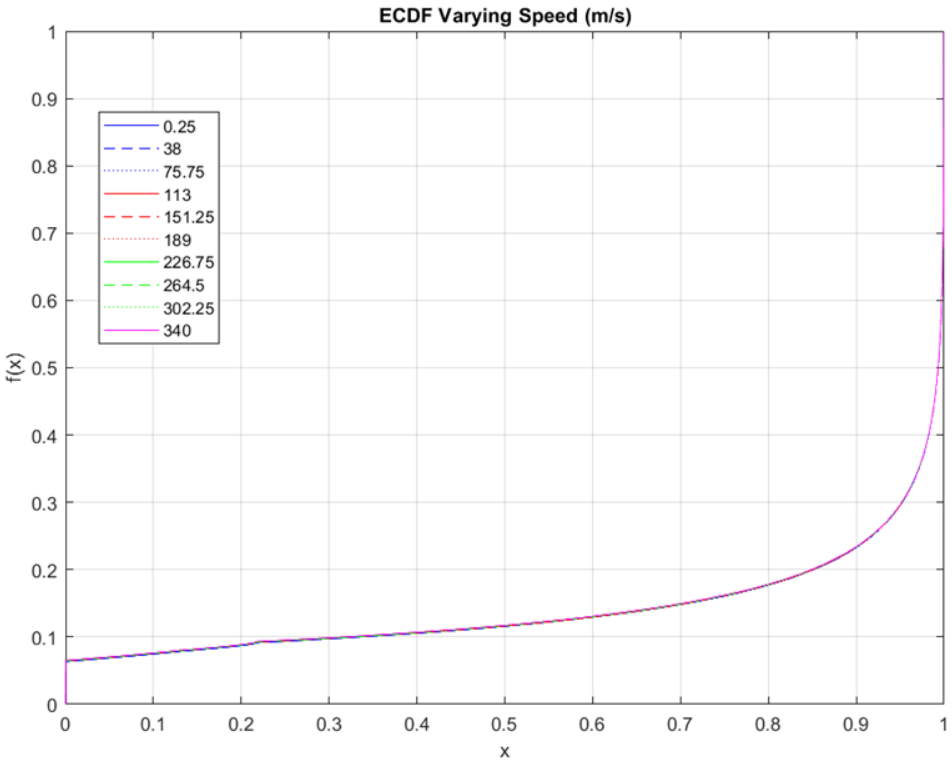

Figure 15. ECDF for Varying Speeds

Reorganizing the data points based on the aircraft speed isolated the variable for observation. The data used to calculate each ECDF curve included every SNR and antenna configuration combination, but only for a given speed. The curves in Figure 15 are indistinguishable, meaning that an aircraft's speed did not have a significant effect on performance. The reason for this is that the speed of light is considerably faster than the aircraft speed, even when approaching Mach 1. Despite the larger difference in aircraft speeds, the round-trip period for the speed of light is too short to allow a meaningful difference in the distance various types of aircraft travel. This is a promising result for implementing mmWave communications systems because it means that, from a speed perspective, they would be appropriate for use with a variety of platforms. Because of the narrow beamwidths associated with mmWaves, there is a small margin for pointing errors. If an aircraft flew fast enough that its displacement significantly affected pointing error, then mmWave communications systems could not function with those platforms. However,

the experiment results indicate that mmWave communication has potential for use on different platforms, ranging from slow moving UAS to high-speed, fixed wing aircraft.

2. Beamwidth

Investigating the relationship between beamwidth and the normalized AF addresses the principal research question. Tighter beamwidths are desirable because they provide high antenna gain to overcome atmospheric attenuation, while inherently lowering the probability of transmitter detection. However, these narrower beams should have a lower tolerance for antenna alignment errors. Figure 16 shows how varying the beamwidth affected performance.

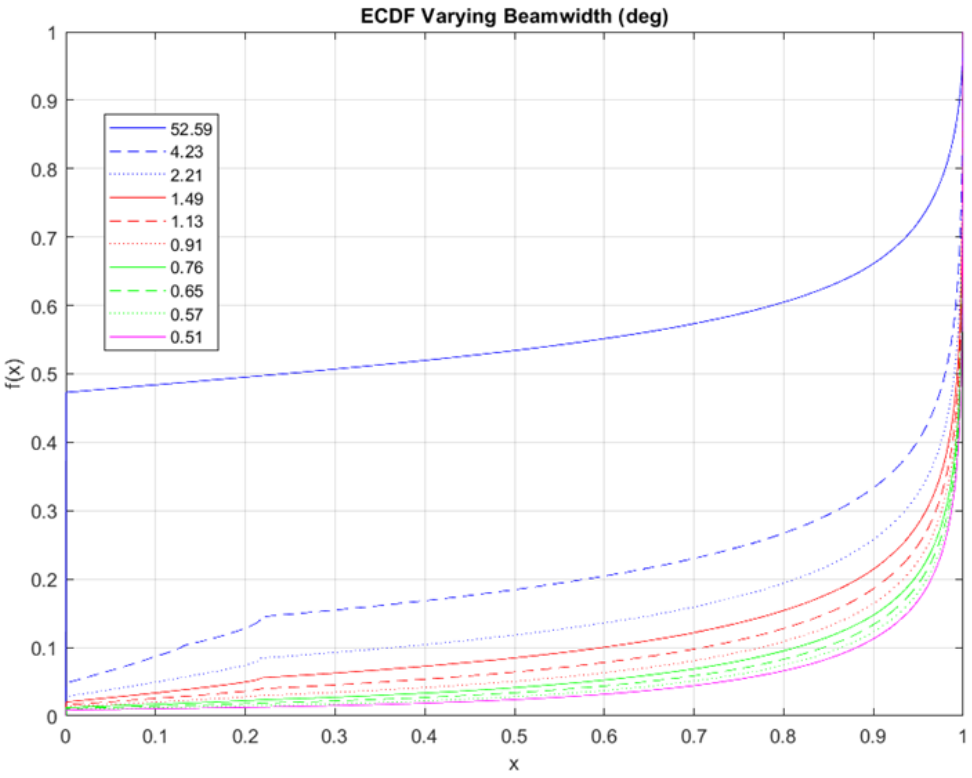

Figure 16. ECDFs for Varying Beamwidths

Like the ECDFs calculated to observe speed, these ECDFs were calculated after isolating N. Therefore, each curve includes data points from every speed and SNR combination. As seen in Figure 16, the results from varying the beamwidth were opposite of what was

anticipated. The simulation results showed that antenna pointing accuracy increased for thinner beamwidths. The projected relationship was that the arrays with wider beamwidths would have better antenna alignment because they have a larger error tolerance. It was also expected that as the beamwidth became narrower there would reach a point where it became too difficult to overcome pointing errors. This expectation did not consider that for ULAs the beamwidth is driven by N. Creating a narrow beam requires increasing N, which in turn increases the AOA estimation accuracy. Therefore, there is not a beamwidth to pointing error trade-space, but rather a mutually beneficial relationship.

3. SNR

The last variable for the experiment was the SNR at the ground station receiver. This SNR directly affects the DOA estimator's ability to approximate the azimuth to the transmitting aircraft. The relationship between performance and SNR is shown in Figure 17.

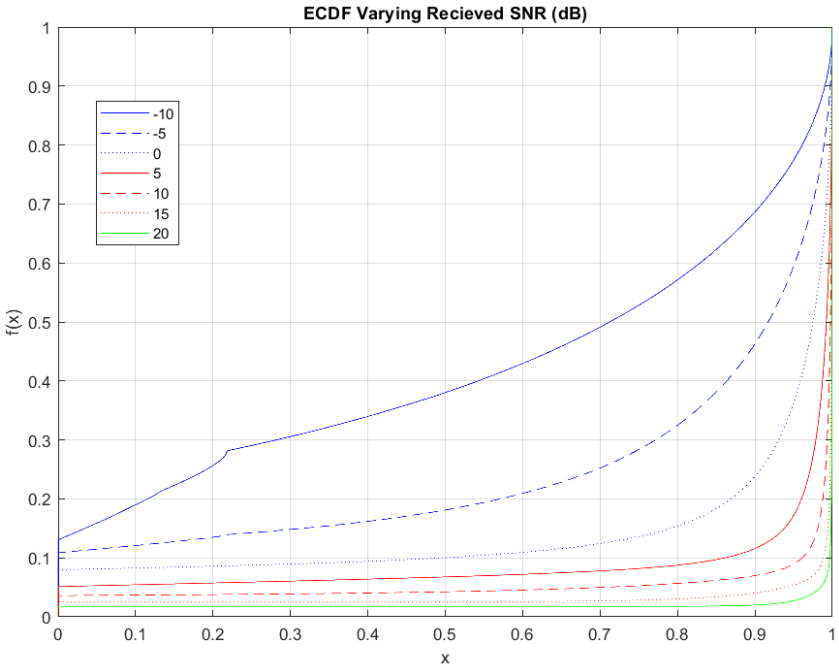

Figure 17. ECDFs for Varying SNR

The curves in Figure 17 reveal that SNR had the greatest impact on performance. As shown, a positive SNR has a nearly 90% probability of resulting in a normalized AF greater than 0.9. The impact of SNR is further demonstrated in Figure 18.

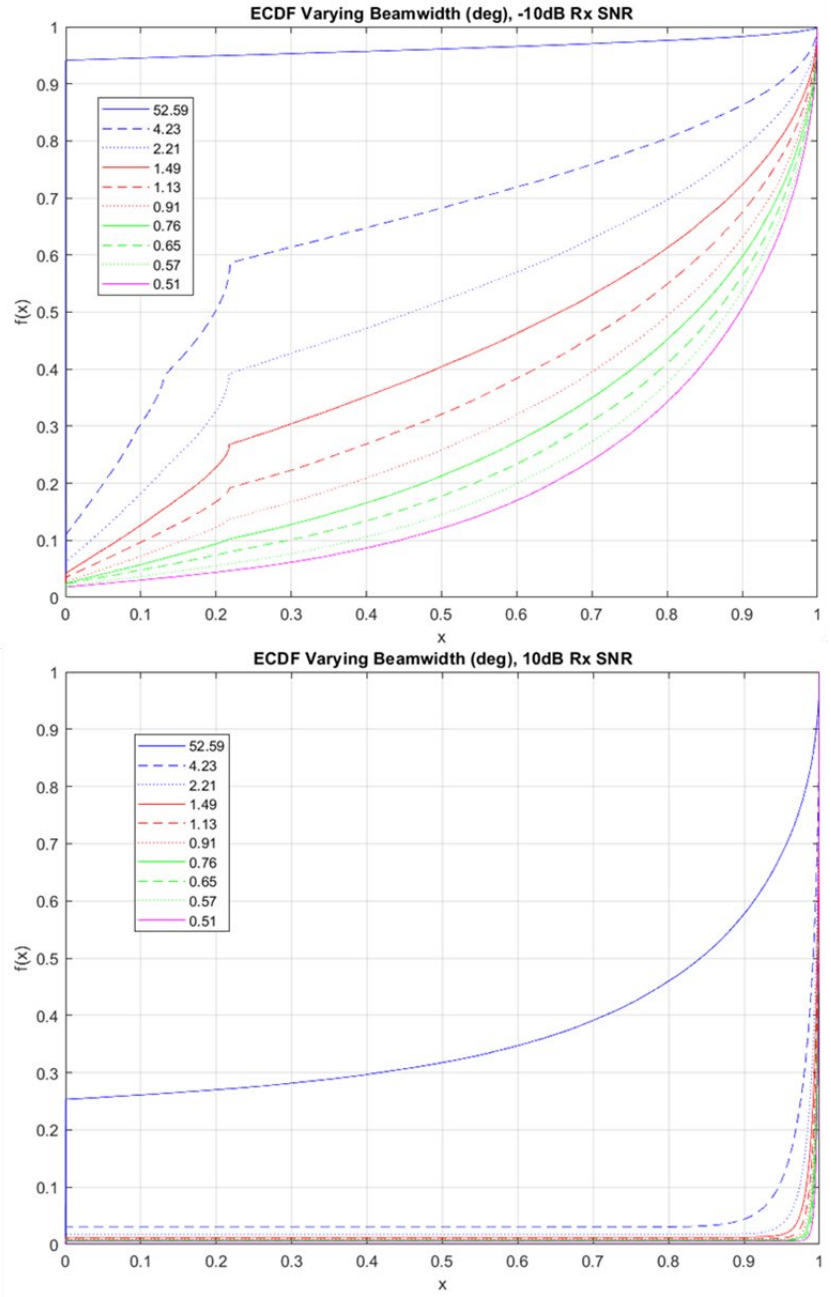

Figure 18. ECDFs for Varying Beamwidth with SNR -10dB Compared to 10 dB

The comparison in Figure 18 shows the ECDFs for different beamwidths, but the top plot includes only trials with a -10dB SNR and the bottom includes only 10dB trials. When compared to the curves from Figure 16, the trials with a lower SNR tend to be less accurate. Conversely, a positive SNR significantly improved antenna pointing accuracy for all antenna lengths. This observation is consistent with sub-space DF theory, which states that a sub-space based estimator should be limited by time and SNR, rather than antenna aperture (Krim & Viberg, 1996).

C. FOLLOW-ON EXPERIMENTATION RESULTS

The initial simulation limited the exploration to using mmWaves in the uplink only, with the assumption that the aircraft would have to use a directionless signal to first contact the ground station. Also, the priority was providing LPD communications for the ground station, so the aircraft could still use an omnidirectional waveform. However, this one-way mmWave-enabled communication would not allow for the aircraft to achieve the same data transfer capabilities as the ground station. Because mmWave communications allow for larger bandwidths, the aircraft using a UHF transmission could not send as much data, as fast as the ground station. Both the ground controller and the aircraft must use mmWave communications to take full advantage of the potential for increased data rates. For this reason, follow-on simulations were conducted to discover how a system would respond when receiving a mmWave carrier frequency, instead of a UHF downlink signal.

As covered in the previous chapter, the follow-on experimentation used a modified simulation design. The simulated ULA for this experiment used 5 mm for both the antenna element size and spacing, which matched the 30 GHz downlink frequency. This change provided the ideal design characteristics for the DOA estimator's ULA performance. The aircraft speed was maintained at 65 m/s for all trials because the initial simulation results revealed that practical aircraft transit speeds did not affect accuracy. Also, the initial results expressed that received SNR had a major impact on performance, so the follow-on simulation expanded the SNR range from -20dB to 20dB. In addition to these changes, the follow-on experimentation observed arrays with fewer elements. This adjustment was made because the initial experiment results demonstrated that pointing accuracy increased

with a larger number of antenna elements. Therefore, the follow-on experimentation aimed to better discern the performance of smaller arrays.

The follow-on experiment results were analyzed with the same method as the initial results. The data points for corresponding to each N value were isolated and used to calculate ECDFs like in the previous experiment. However, the aircraft speed did not change in this situation, so each data point has an associated speed of 65 m/s. The ECDF calculations still included all the received SNRs for a given N, which are plotted together in Figure 19.

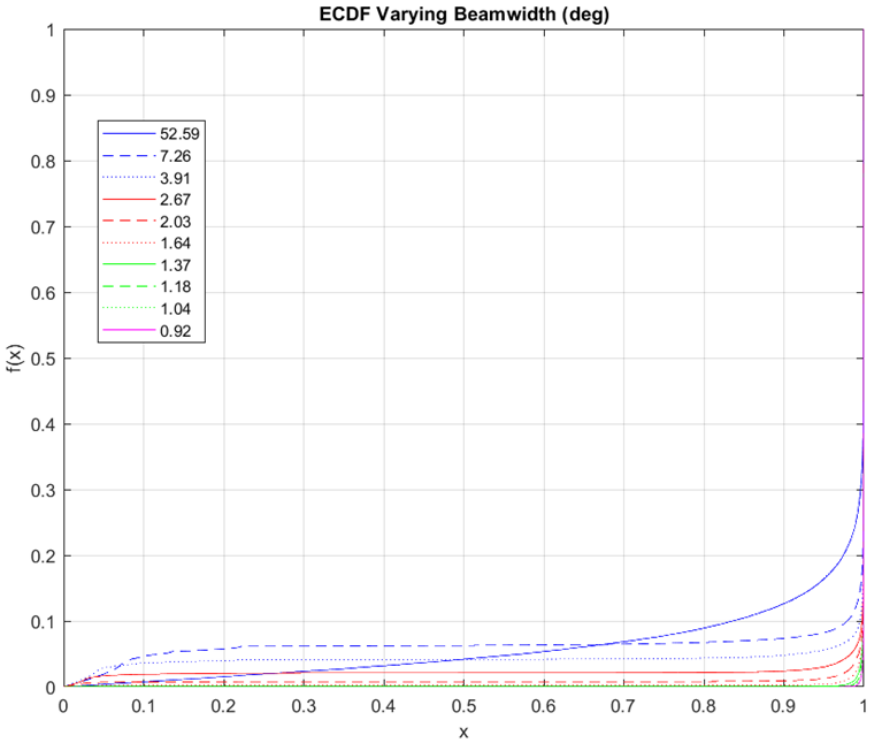

Figure 19. ECDFs for Varying Beamwidths, Two-Way mmWave System

As shown, the curves in Figure 19 and flatter than the curves in Figure 16. This behavior indicates that a communication system using mmWaves in both directions could achieve more accurate DOA estimates than just using a mmWave uplink. This is due to the increased downlink frequency and the ULA element spacing. The ground station ULA was designed to transmit at mmWave frequencies, so it placed the elements 5 mm apart,

idealized for the 30 GHz transmission. For the one-way mmWave experiment, the ULA received a 300 MHz signal, but the antenna element spacing was still configured for higher frequencies. The antenna elements would have needed to be placed 0.5 m apart for ideal spacing in the initial scenario. As a consequence, the initial experiment design used a ULA designed to transmit mmWaves but received a UHF signal, which limited the performance. Conversely, the DOA estimator, for the follow-on experimentation, used a half-wavelength element spacing that matched the received carrier frequency, which produced ideal performance . When using a two-way mmWave link, the simulated ULA was designed with both ideal antenna element length and spacing, resulting in superior signal reception.

The simulation using a mmWave downlink outperformed the experiment using a 300 MHz downlink for similar antenna lengths. Table 4 shows the difference between the average AF for similar antenna configurations when using a UHF downlink versus a mmWave downlink. The mean AFs for the two-way mmWave experiment are noticeably higher.

Table 4. Comparison of Mean AF.

N, UHF	Mean AF, UFH	N, mmWave	Mean AF, mmWave
2	0.4426	2	0.9429
46	0.8572	50	0.991
90	0.9228	86	0.9996
112	0.9326	110	0.9998

The results from this simulation show a similar trend to the previous iteration, with the accuracy generally increasing with array length. However, there is a difference with the shortest array. In the original simulation, the shortest array often resulted in a complete miss or poor accuracy. In the mmWave downlink scenario, the shortest array still resulted in relatively poor accuracy, but it outperformed some longer array configurations at lower AF ratios. This suggests that when using a mmWave downlink, arrays with wider beamwidths will have fewer complete pointing misses but may still struggle to achieve precise antenna alignment. In addition to the different behavior from the shortest array, the mmWave downlink simulation results show greater antenna pointing accuracy overall.

Also, the follow-on experiment resulted in increased performance for shorter arrays. This improved performance led to the final experiment to gain greater fidelity at shorter array lengths.

The final experiment was conducted in the same manner as the previous one, but with the antenna configurations in Table 3. Figure 20 shows the ECDFs resulting from using these parameters.

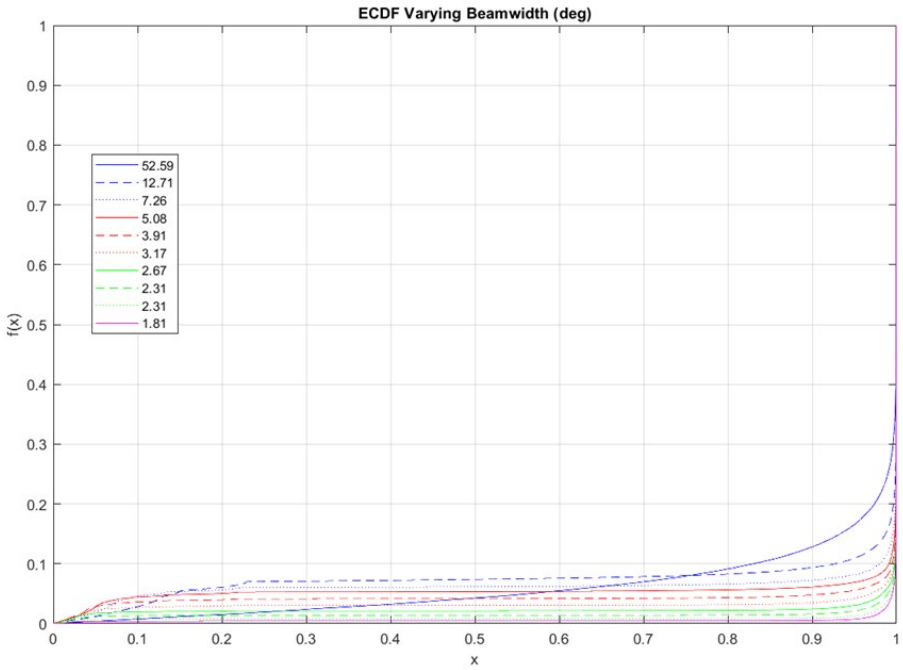

Figure 20. ECDFs for Varying Beamwidths, Two-Way mmWave System, Short Antennas

The results in Figure 20 reflect what was also shown in Figure 19. The two-element array remains the only antenna that does not follow the same general performance pattern. Also based on the ECDFs, every antenna with at least eight elements should achieve an AF or 0.9 approximately 90% of the time. Starting with the eight-element array, the performance improves consistently with increasing array length.

The relationship between SNR and antenna alignment for the follow-on experimentation was like the original simulations results. However, the accuracy at lower SNRs increased as shown in Figure 21.

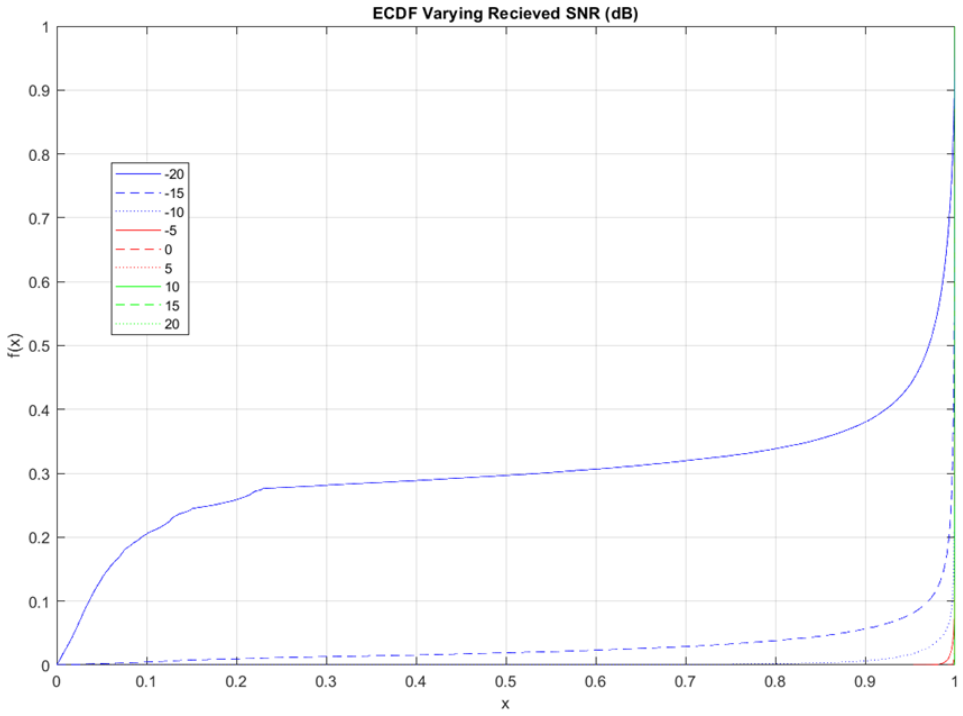

Figure 21. ECDFs for Varying SNR, Two-Way mmWave System, Short Antennas

Because the antenna DOA estimation capability improved with the mmWave downlink scenario, the estimates were more accurate at lower SNRs. As seen in Figure 21, there were virtually no antenna alignment errors when the ground station received a positive SNR. This result reinforced the importance of the receiver's SNR in estimating the transmitters position and achieving precise antenna alignment.

D. ANALYSIS OF IMPACT ON SYSTEMS

The simulation results provide insight on the potential for implementing mmWave communication systems for aviation C2 and the critical engineering characteristics for their design. First, the simulated system performance was consistent for all aircraft speeds. This

result suggests using DOA estimation as a method for maintaining antenna alignment is appropriate for different aircraft types. Having a single system with the flexibility to communicate with aircraft the fly at different speeds is necessary because aviation C2 units must manage airspace that include a range of platforms. A mmWave communication system with an antenna that supports DOA estimation could provide a ground station with the capabilities necessary to communicate with aircraft moving through space.

In addition to the encouraging results from speed analysis, the simulated mmWave communication was not limited by beamwidth, as it was expected to be. This research's primary objective was to discover the trade-space between narrowing beamwidth and the effort required aligning antennas. However, the experiment results revealed that achieving a narrower beamwidth increased antenna pointing accuracy because both are directly correlated to N. This result also indicated that there is not an ideal beamwidth because pointing accuracy increased along with creating thinner beams. Therefore, when using DOA estimates to align mmWave antennas, the limiting factor is the array length, rather than the signal's beamwidth. Array length is constrained by cost and space available for deployment. Designing a longer array would require increasing N, so the maximum desirable length would depend on the cost to produce or acquire the individual antenna elements. Also, the physical space an array occupies restricts its maximum length. This limitation is amplified for a two-way mmWave communication design because of size, weigh, and power considerations when integrating systems onto an aircraft.

Although using a two-way mmWave datalink may limit antenna size for aircraft, the simulation showed that shorter antennas performed better when using the higher frequency. The ULA was optimized to use mmWave frequency, so the DOA estimation significantly increased, despite the arrays having fewer elements. Designing a system that used mmWave communications for both the aircraft and the ground station would help mitigate potential array length limitations. Additionally, the concept behind using mmWaves for the uplink only was to provide the ground station protection through LPD communications, while reducing the need to align antennas in both directions. However, using a two-way mmWave datalink resulted in a significant increase in pointing accuracy. This superior performance implies that using mmWaves in both directions would provide

better antenna alignment, given that there is a technique developed for initial acquisition. Also, using a two-way mmWave datalink would prevent issues caused by transmitting and receiving on different frequencies.

The simulation results identified SNR as the parameter with the largest impact on a system's ability to maintain antenna alignment. For both the mmWave uplink only and bidirectional mmWave iterations, increasing the SNR enhanced the DOA estimator's ability to accurately approximate an aircraft's azimuth. When using mmWave for the uplink only, the estimator required a positive SNR to achieve consistent accuracy. Conversely, the two-way mmWave system regularly produced accurate estimations even at some negative SNRs. The implications for systems design are that SNR is a limiting factor for performance. The system should be designed to maximize power output, antenna gain, and receiver sensitivity. The mmWave communication system's range will depend on the available technologies capabilities to minimize signal power loss over distance. Also, pointing accuracy contributes to SNR because more power will reach the receiver when antennas are properly aligned. This again highlights the need for initial acquisition techniques because the first received SNR will directly impact the accuracy of follow-on transmissions.

THIS PAGE INTENTIONALLY LEFT BLANK

V. CONCLUSION

A. SUMMARY

The inspiration for this thesis was to propose a technical solution to the SIGMAN challenge that Marine aviation C2 units face. This research explored if mmWaves could provide a LPD waveform, while still supporting aviation communication needs. Chapter II reviewed existing literature about USMC C2 needs, 5G, and mmWave aviation applications. Potential adversaries threaten Marine aviation C2 nodes with developing DF capabilities and long range, precision fires. Current SIGMAN tactics do not provide adequate defense against emerging threats. Evolving 5G technology shows potential for military applications because it can provide higher data rates and LPD communications with mmWaves. However, mmWave communications systems must use PAT techniques to sustain proper antenna alignment, for moving vehicle applications. This thesis used a simulation to explore the beam steering and antenna alignment challenge.

Chapter III discussed the experiment methodology, and Chapter IV presented the simulation results. The simulation used Monte Carlo trials to discover how aircraft speed, received SNR, and transmitted signal's beamwidth affected a ULA's DOA estimation capability. The DOA estimation directly links to antenna pointing accuracy. To measure performance, the simulation used the normalized AF achieved in each situation. Inputting the calculated AFs into a series of ECDF, provided a method of comparing performance based on different variables. The initial experiment used an UHF downlink and a mmWave uplink and the results revealed that the received SNR had the greatest impact on estimation accuracy. The follow-on experiment simulated mmWaves for both the uplink and the downlink because a bidirectional datalink would be required to achieve the full benefits from utilizing mmWaves. The follow-on experiment design used the information obtained from the initial simulation to focus on the effects of SNR and performance using shorter array lengths. When the DOA estimator received a mmWave downlink signal, the accuracy improved significantly, even at lower SNRs, because the 5mm antenna element spacing for the simulated ULA matched the received a 30 GHz operating frequency. Even though in the initial ULA simulated ideal sized antenna elements, the 5 mm element spacing was

much shorter than the ideal half-wavelength for a 300 MHz signal (0.5 m), which lowered performance.

B. CONCLUSIONS

The primary research question for this thesis asked about the trade-space between creating a narrower signal beamwidth and maintaining proper antenna alignment. The experiment results revealed that there is not a trade-space between beamwidths used in this simulation and antenna alignment, but that there is a beneficial relationship. If the antenna beams needed to be exceptionally thin, then there may be a point where even small pointing errors prevent proper antenna alignment. In this experiment, both the beamwidth and DOA estimator accuracy were dependent on the number of array antenna elements. When the number of antenna elements increased, to narrow the beamwidth, the DOA estimate improved. This result also answered the secondary research question, which asked if there is an optimal beamwidth for mmWave communications. Because the simulation demonstrated that there is no trade-off, beamwidth should not limit engineering designs. In addition to answering the research questions, the experiment results highlighted the importance of the received SNR and showed that a bidirectional mmWave communication link outperformed a one-way system. In the bidirectional situation, the DOA estimator's ULA had used 5 mm for both the antenna element size and spacing, which achieved ideal performance with the received a 30 GHz signal. The received SNR had the largest impact on pointing accuracy, which implies that limiting noise within a mmWave communications system is critical. Also, the follow-on experiment exhibited that the DOA estimator's accuracy increased when it received a mmWave frequency downlink, rather than a UHF downlink. This result suggests that having both the ground station and the aircraft use mmWave transmissions will provide the most accuracy, while also enabling rapid data transfer in both directions. The answers to the research questions and the additional findings from this thesis imply that the cost of antenna elements and the ability to minimize system noise are the limiting factors for mmWave communications system design.

This thesis showed that array antennas can use beamforming to make narrow signal beams, while using DF capabilities to accurately aim signals. Also, for practical transit

speeds, aircraft velocity does not affect system performance, so a mmWave communications system can support C2 with multiple types of platforms. The results demonstrated that arrays with as few as 8 elements, or 4 cm in length, perform with consistent accuracy. These small array sizes should create flexibility for integration into potential systems. This thesis research showed that mmWave communication systems have the potential to support future aviation C2 requirements.

C. RECOMMENDATIONS FOR FUTURE RESEARCH

Future research related to this thesis should explore commercially available 5G array antenna performance, a more detailed technique for signal maintenance, and initial signal acquisition strategies. Experimenting with existing 5G array antennas would provide a better understanding of the achievable beamwidths and range limitations for mmWave communications. The simulation for this research used DOA estimation as the basis for antenna pointing. Studying computational requirements to perform DOA calculations and subsequent beam steering would provide further understanding of the effort required during consistent communication. Finally, this research found that a bidirectional mmWave signal provided the best performance. For a system like this to succeed, the aircraft would need a method to establish initial contact with the ground station. Examining initial access strategies and potentially amplifying beam tracking with platform position information would contribute to developing vehicular mmWave communications.

THIS PAGE INTENTIONALLY LEFT BLANK

APPENDIX. MATLAB SCRIPTS

A. INITIAL EXPERIMENT

```
%Evaluating the Feasibility of 5G Enabled Datalinks for Aviation Command and Control
%Experiment
%Brian White
%Naval Postgraduate School
%June 2021
%Simulation creates an 1000 aircraft each with a random initial postion and
%trajectory within a 50x50km area. Aircraft speed, antenna lenght, and SNR
%are varried to observe how each effects antenna beamforming pointing error
%based on the aircraft position off boresight. 10 samples are collected at
%a 6 second interval representing 1 minute of collection.

clear
clc
close all
warning('off','all') %supress warnings from when estimator doen't get enough DOAs
warning
%% Constants
Tstep = 6; %time step
xdist = 50e3; % horizontal distance traveled (length of Okinawa)
c= physconst('LightSpeed');
dascPos = [0;0;0]; %DASC pos
dasc = phased.Platform('InitialPosition',dascPos); %defeine DASC
%reciever
t= (0:1/1200:1); %fs= 1200
data= 300; %frequency of unmodulated transmission
sinWave= cos(2*pi*t*data); %sinusoidal waveform
%transmitter
space= 0.5; %half wavelength element spacing
fc= 30e9; %mmwave tx carrier frequency
lambda= c/fc; %wavelength
d= space*lambda;
%% Simulation Parametrs
%simulation space
speed= linspace(0.25,340,10);%lower bound for speed from UAS to approx mach 1
N = linspace(2,110,10);%number of elements
snr= -10:5:20; %snr range in dB
sticks= 1000; %1000
%Tx antenna metrics
L=N*d; %length ULA
HP_rad= 2*asin(0.443*lambda./L); %HPBW calculation
```

```
HP= rad2deg(HP_rad);
%% Simulation

stoSpeed= cell(length(speed),1); %preallocation for final data storage
%%%nested Loops%%%
tic

%1. SELECT A/C SPEED GATE
for s= 2:length(speed)
cruise= speed(s);

%2. SELECT NUMBER OF ANTENNA ELEMENTS
stoN= cell(length(N),1);
for n= 1:length(N)
%Create ULA
ant = phased.ULA('NumElements',N(n),...%ULA with N elements, default
'ElementSpacing', d);%half wavelength spacing

%Rx
estimator = phased.RootMUSICEstimator('SensorArray',ant,...
'NumSignalsSource','Property',...
'NumSignals',1); %default operating freq 3e8 Hz

%3. SELECT Rx SNR
stoSNR= cell(length(snr),1);
for q= 1:length(snr)
Nsteps= 10; %10 time steps
pattrnMat= zeros(sticks, Nsteps); %preallocate array pattern storage
for traj= 1:sticks
%random initial position
ypos = -1*(xdist/2) + 2*(xdist/2)*rand(1,1); %uniformly distributed random y positions
xpos = -1*(xdist/2) + 2*(xdist/2)*rand(1,1); %uniformly distributed random y positions
initPos= [xpos;ypos;0]; %random starting position in 50 km square
rTheta= rand(1,1);
theta= -90 +(2*90)*rTheta; %uniform random trajectroy between -90 and 90 degrees
cruiseX= cruise*cosd(theta); %velocity in x
cruiseY= cruise*sind(theta); %velocity in y
initVel(1)= cruiseX; %m/s
initVel(2)= cruiseY;
initVel(3)= 0; %ignoring altitude

plane = phased.Platform('InitialPosition',initPos,'Velocity',initVel'); %define a/c with
initial pos and vel

posmat = zeros(3,Nsteps); %preallocate vector for a/c position
```

```
azimuthmat= zeros(1, Nsteps); %vector of real azimuth
elevmat= zeros(1, Nsteps); %vector of real elevation
azmat= zeros(1, Nsteps); %vector of estimated elevation
estAoAMat= zeros(1, Nsteps); %vector for estimated angle
realAoAMat= zeros(1, Nsteps); %vector for actual angle
normAFMat= zeros(1, Nsteps); %vector normalized AF
disp= zeros(3, Nsteps); %vector to store a/c pos after transmisions
distmat= zeros(1,Nsteps); %vector for a/c distance

for k = 1:Nsteps
pos = plane(Tstep);
posmat(:,k) = pos; %store postion in vector
[azimuth,elevation,dist] = cart2sph(pos(1),pos(2),pos(3)); %convert rectangular location
to spherical coordinates
azim= rad2deg(azimuth); %actual a/c initial azimuth
%this azimuth is measured counter clockwise from the positive x axis
elev= rad2deg(elevation);
azimuthmat(:,k)= azim; %store angle of arrival
elevmat(:,k)=elev; %store elevation in degrees
distmat(:,k)=dist;
%%%Esitmate angle of arrival
ang= [azim;elev]; %make angle input for plane wave function
wave= collectPlaneWave(ant,sinWave',ang); %plane wave
signal= awgn(wave, snr(q)); %add noise to signanl
estAoA= estimator(signal); %estimated AoA
estAoAMat(:,k)= estAoA;
%Estimated azimuth is measured in the most direct
%direction from the x axis (0 degrees off of boresight for the ULA)
%%%Calculate A/C Displacement for signal round trip
dispTime= (dist/c)*2; %round trip time for Rx and Tx signal
dispX= cruiseX(1)*dispTime; %distanced traveld during rnd trip time
dispY= cruiseY(1)*dispTime;
disp(:,k)= [pos(1)+dispX; pos(2)+dispY; pos(3)]; %add x and y movement to find actual
a/c pos
[newAzimuth,newElevation,newDist] = cart2sph(disp(1,k),disp(2,k),disp(3,k));
newAzim= rad2deg(newAzimuth); %actual a/c final azimuth
%this azimuth is measured counter clockwise from the positive x axis
newElev= rad2deg(newElevation);
realAoA= az2broadside(newAzim);
%Need to change azimuth measured counter clockwise from
%x to match the estimated angle.
realAoAMat(:,k)= realAoA;
%%%Find normalized AF based on BW from pointing angle and receiver at actual angle
u= sind(realAoA); %determine where beam hits reciever
up= sind(estAoA); %determines "pointed" beam pattern
```

```
normAF= abs(sin(N(n)*pi/2*(u-up))/(N(n)*sin(pi/2*(u-up))));
%Normalized AF represents % of power transmitted to
%reciever. Take absolute value in case Rx in sidelobe.
normAFMat(:,k)= normAF;
end

pattrnMat(traj,:)= normAFMat; %saves data for 1 epoch
stoSNR{q,:}= pattrnMat;%stores data for snr trials
end

stoN{n,:}= stoSNR; %stores data for antenna configurations
end
stoSpeed{s,:}= stoN; %stores data for all data in speed trials
end

end

toc
```

B. FOLLOW-ON EXPERIMENT

```
%Evaluating the Feasibility of 5G Enabled Datalinks for Aviation Command and Control
%Follow-on Experiment
%Brian White
%Naval Postgraduate School
%June 2021
%Simulation creates an 1000 aircraft each with a random initial postion and
%trajectory within a 50km area. Aircraft speed, antenna lenght, and SNR
%are varried to observe how each effects antenna beamforming pointing error
%based on the aircraft position off boresight. 10 samples are collected at
%a 6 second interval representing 1 minute of collection.

clear
clc
close all
warning('off','all') %supress warnings from when estimator doen't get enough DOAs
warning
%% Constants
Tstep = 6; %time step
xdist = 50e3; % horizontal distance traveled (length of Okinawa)
c= physconst('LightSpeed');
dascPos = [0;0;0]; %DASC pos
dasc = phased.Platform('InitialPosition',dascPos); %defeine DASC
%reciever
t= (0:1/1200:1); %fs= 1200
```

```
data= 300; %frequency of unmodulated transmission
sinWave= cos(2*pi*t*data); %sinusoidal waveform
%transmitter
space= 0.5; %half wavelength element spacing
fc= 30e9; %mmwave tx carrier frequency
lambda= c/fc; %wavelength
d= space*lambda;
%% Simulation Parametrs
%simulation space
speed= 65;%lower bound for speed from UAS to approx mach 1
N = linspace(2,110,10);%number of elements
snr= -20:5:20; %snr range in dB
sticks= 1000; %1000
%Tx antenna metrics
L=N*d; %length ULA
HP_rad= 2*asin(0.443*lambda./L); %HPBW calculation
HP= rad2deg(HP_rad);
%% Simulation
stoSpeed= cell(length(speed),1); %preallocation for final data storage
%%%nested Loops%%%
tic
cruise= speed;
%1. SELECT NUMBER OF ANTENNA ELEMENTS
stoN= cell(length(N),1);
for n= 1:length(N)
%Create ULA
ant = phased.ULA('NumElements',N(n),...%ULA with N elements, default
'ElementSpacing', d);%half wavelength spacing

ant.Element.FrequencyRange = [25e9 35e9];

%Rx
estimator = phased.RootMUSICEstimator('SensorArray',ant,...
'OperatingFrequency', fc,'NumSignalsSource','Property',...
'NumSignals',1); %%operating freq as 30 GHz carrier

%2. SELECT Rx SNR
stoSNR= cell(length(snr),1);
for q= 1:length(snr)
Nsteps= 10; %10 time steps
pattrnMat= zeros(sticks, Nsteps); %pre allocate array pattern storage
for traj= 1:sticks
%random initial position
ypos = -1*(xdist/2) + 2*(xdist/2)*rand(1,1); %uniformly distributed random y positions
xpos = -1*(xdist/2) + 2*(xdist/2)*rand(1,1); %uniformly distributed random y positions
```

```
initPos= [xpos;ypos;0]; %random starting position in 50 km square
rTheta= rand(1,1);
theta= -90 +(2*90)*rTheta; %uniform random trajectroy between -90 and 90 degrees
cruiseX= cruise*cosd(theta); %velocity in x
cruiseY= cruise*sind(theta); %velocity in y
initVel(1)= cruiseX; %m/s
initVel(2)= cruiseY;
initVel(3)= 0; %ignoring altitude

plane = phased.Platform('InitialPosition',initPos,'Velocity',initVel'); %define a/c with initial pos and vel

posmat = zeros(3,Nsteps); %preallocate vector for a/c position
azimuthmat= zeros(1, Nsteps); %vector of real azimuth
elevmat= zeros(1, Nsteps); %vector of real elevation
azmat= zeros(1, Nsteps); %vector of estimated elevation
estAoAMat= zeros(1, Nsteps); %vector for estimated angle
realAoAMat= zeros(1, Nsteps); %vector for actual angle
normAFMat= zeros(1, Nsteps); %vector normalized AF
disp= zeros(3, Nsteps); %vector to store a/c pos after transmisions
distmat= zeros(1,Nsteps); %vector for a/c distance

for k = 1:Nsteps
pos = plane(Tstep);
posmat(:,k) = pos; %store postion in vector
[azimuth,elevation,dist] = cart2sph(pos(1),pos(2),pos(3)); %convert rectangular location to spherical coordinates
azim= rad2deg(azimuth); %actual a/c initial azimuth
%this azimuth is measured counter clockwise from the positive x axis
elev= rad2deg(elevation);
azimuthmat(:,k)= azim; %store angle of arrival
elevmat(:,k)=elev; %store elevation in degrees
distmat(:,k)=dist;
%%%Esitmate angle of arrival
ang= [azim;elev]; %make angle input for plane wave function
wave= collectPlaneWave(ant,sinWave',ang, fc); %plane wave
signal= awgn(wave, snr(q)); %add noise to signanl
estAoA= estimator(signal); %estimated AoA
estAoAMat(:,k)= estAoA;
%Estimated azimuth is measured in the most direct
%direction from the x axis (0 degrees off of boresight for the ULA)
%%%Calculate A/C Displacement for signal round trip
dispTime= (dist/c)*2; %round trip time for Rx and Tx signal
dispX= cruiseX(1)*dispTime; %distanced traveld during rnd trip time
dispY= cruiseY(1)*dispTime;
```

```
disp(:,k)= [pos(1)+dispX; pos(2)+dispY; pos(3)]; %add x and y movement to find actual
a/c pos
[newAzimuth,newElevation,newDist] = cart2sph(disp(1,k),disp(2,k),disp(3,k));
newAzim= rad2deg(newAzimuth); %actual a/c final azimuth
%this azimuth is measured counter clockwise from the positive x axis
newElev= rad2deg(newElevation);
realAoA= az2broadside(newAzim);
%Need to change azimuth measured counter clockwise from
%x to match the estimated angle.
realAoAMat(:,k)= realAoA;
%%%Find normalized AF based on BW from pointing angle
%%%and receiver at actual angle
u= sind(realAoA); %determine where beam hits reciever
up= sind(estAoA); %determines "pointed" beam pattern
normAF= abs(sin(N(n)*pi/2*(u-up))/(N(n)*sin(pi/2*(u-up))));
%Normalized AF represents % of power transmitted to
%reciever. Take absolute value in case Rx in sidelobe.
normAFMat(:,k)= normAF;

end

pattrnMat(traj,:)= normAFMat; %saves data for 1 epoch
stoSNR{q,:}= pattrnMat;%stores data for snr trials
end

stoN{n,:}= stoSNR; %stores data for antenna configurations
end

end
toc
```

C. ECDF GENERATION

```
%Evaluating the Feasibility of 5G Enabled Datalinks for Aviation Command and Control
%ECDF Plots
%Brian White
%Naval Postgraduate School
%June 2021
%Isolates each variable from the Monte Carlo trials.
%Calculates and plots ECDFs.
%%
clear
clc
close all
load('thesisData')
```

```
%% Speed ECDF
a=1;
c=1;
e=1;
for a= 1:10
for c= 1:10
for e= 1:7
new= vertcat(stoSpeed{a, 1}{c, 1}{e, 1}(:));
newMat(:,e)= new;
end
newE(:,c)= vertcat(newMat(:));
end
final(:,a)= vertcat(newE(:));

end
final(isnan(final))= 0;

figure(1)
[f1,x1]= ecdf(final(:,1));
plot(x1, f1, '-b')
hold on
[f2,x2]= ecdf(final(:,2));
plot(x2, f2, '--b')
[f3,x3]= ecdf(final(:,3));
plot(x3, f3, ':b')
[f4,x4]= ecdf(final(:,4));
plot(x4, f4, '-r')
[f5,x5]= ecdf(final(:,5));
plot(x5, f5, '--r')
[f6,x6]= ecdf(final(:,6));
plot(x6, f6, ':r')
[f7,x7]= ecdf(final(:,7));
plot(x7, f7, '-g')
[f8,x8]= ecdf(final(:,8));
plot(x8, f8, '--g')
[f9,x9]= ecdf(final(:,9));
plot(x9, f9, ':g')
[f10,x10]= ecdf(final(:,10));
plot(x10, f10, 'm')
title('ECDF Varying Speed (m/s)')
xlabel('x')
ylabel('f(x)')
legend('0.25', '38', '75.75', '113', '151.25', '189', '226.75',...
'264.5', '302.25', '340')
grid
```

```
set(gcf,'color','white')
hold off

%% Antenna ECDF
a=1;
c=1;
e=1;
for c= 1:10
for a= 1:10
for e= 1:7
new= vertcat(stoSpeed{a, 1}{c, 1}{e, 1}(:));
newMat(:,e)= new;
end
newE2(:,a)= vertcat(newMat(:));
end
finalN(:,c)= vertcat(newE2(:));

end
finalN(isnan(finalN))= 0;
figure(2)
[f1,x1]= ecdf(finalN(:,1));
plot(x1, f1, '-b')
hold on
[f2,x2]= ecdf(finalN(:,2));
plot(x2, f2, '--b')
[f3,x3]= ecdf(finalN(:,3));
plot(x3, f3, ':b')
[f4,x4]= ecdf(finalN(:,4));
plot(x4, f4, '-r')
[f5,x5]= ecdf(finalN(:,5));
plot(x5, f5, '--r')
[f6,x6]= ecdf(finalN(:,6));
plot(x6, f6, ':r')
[f7,x7]= ecdf(finalN(:,7));
plot(x7, f7, '-g')
[f8,x8]= ecdf(finalN(:,8));
plot(x8, f8, '--g')
[f9,x9]= ecdf(finalN(:,9));
plot(x9, f9, ':g')
[f10,x10]= ecdf(finalN(:,10));
plot(x10, f10, 'm')
title('ECDF Varying Beamwidth (deg)')
xlabel('x')
ylabel('f(x)')
legend('52.59', '4.23', '2.21', '1.49', '1.13', '0.91', '0.76',...
```

```
‘0.65’, ‘0.57’, ‘0.51’)
grid
set(gcf,’color’,’white’)
hold off
%% SNR ECDF
a=1;
c=1;
e=1;
for e= 1:7
for a= 1:10
for c= 1:10
new= vertcat(stoSpeed{a, 1}{c, 1}{e, 1}(:));
newMatC(:,c)= new;
end
newA(:,a)= vertcat(newMatC(:));
end
finalSNR(:,e)= vertcat(newA(:));

end
finalSNR(isnan(finalSNR))= 0;
figure(3)
[f1,x1]= ecdf(finalSNR(:,1));
plot(x1, f1, ‘-b’)
hold on
[f2,x2]= ecdf(finalSNR(:,2));
plot(x2, f2, ‘--b’)
[f3,x3]= ecdf(finalSNR(:,3));
plot(x3, f3, ‘:b’)
[f4,x4]= ecdf(finalSNR(:,4));
plot(x4, f4, ‘-r’)
[f5,x5]= ecdf(finalSNR(:,5));
plot(x5, f5, ‘--r’)
[f6,x6]= ecdf(finalSNR(:,6));
plot(x6, f6, ‘:r’)
[f7,x7]= ecdf(finalSNR(:,7));
plot(x7, f7, ‘-g’)
title(‘ECDF Varying Recieved SNR (dB)’)
xlabel(‘x’)
ylabel(‘f(x)’)
legend(‘-10’, ‘-5’, ‘0’, ‘5’, ‘10’, ‘15’, ‘20’)
grid
set(gcf,’color’,’white’)
hold off

%% -10dB SNR with all N ECDF
```

```
a=1;
c=1;
e=1;
for c=1:10
for a= 1:10
newI= vertcat(stoSpeed{a, 1}{c, 1}{e, 1}(:));
newiMat(:,a)= newI;
end
finalIdeal(:,c)= vertcat(newiMat(:));
end
finalIdeal(isnan(finalIdeal))= 0;
figure(4)
[f1,x1]= ecdf(finalIdeal(:,1));
plot(x1, f1, '-b')
hold on
[f2,x2]= ecdf(finalIdeal(:,2));
plot(x2, f2, '--b')
[f3,x3]= ecdf(finalIdeal(:,3));
plot(x3, f3, ':b')
[f4,x4]= ecdf(finalIdeal(:,4));
plot(x4, f4, '-r')
[f5,x5]= ecdf(finalIdeal(:,5));
plot(x5, f5, '--r')
[f6,x6]= ecdf(finalIdeal(:,6));
plot(x6, f6, ':r')
[f7,x7]= ecdf(finalIdeal(:,7));
plot(x7, f7, '-g')
[f8,x8]= ecdf(finalIdeal(:,8));
plot(x8, f8, '--g')
[f9,x9]= ecdf(finalIdeal(:,9));
plot(x9, f9, ':g')
[f10,x10]= ecdf(finalIdeal(:,10));
plot(x10, f10, 'm')
title('ECDF Varying Beamwidth (deg), -10dB Rx SNR')
xlabel('x')
ylabel('f(x)')
legend('52.59', '4.23', '2.21', '1.49', '1.13', '0.91', '0.76',...
'0.65', '0.57', '0.51')
grid
set(gcf,'color','white')
hold off
%% 10dB SNR with all N ECDF
a=1;
c=1;
e=5;
```

```
for c=1:10
for a= 1:10
newI= vertcat(stoSpeed{a, 1}{c, 1}{e, 1}(:));
newiMat(:,a)= newI;
end
finalIdeal(:,c)= vertcat(newiMat(:));
end
finalIdeal(isnan(finalIdeal))= 0;
figure(5)
[f1,x1]= ecdf(finalIdeal(:,1));
plot(x1, f1, '-b')
hold on
[f2,x2]= ecdf(finalIdeal(:,2));
plot(x2, f2, '--b')
[f3,x3]= ecdf(finalIdeal(:,3));
plot(x3, f3, ':b')
[f4,x4]= ecdf(finalIdeal(:,4));
plot(x4, f4, '-r')
[f5,x5]= ecdf(finalIdeal(:,5));
plot(x5, f5, '--r')
[f6,x6]= ecdf(finalIdeal(:,6));
plot(x6, f6, ':r')
[f7,x7]= ecdf(finalIdeal(:,7));
plot(x7, f7, '-g')
[f8,x8]= ecdf(finalIdeal(:,8));
plot(x8, f8, '--g')
[f9,x9]= ecdf(finalIdeal(:,9));
plot(x9, f9, ':g')
[f10,x10]= ecdf(finalIdeal(:,10));
plot(x10, f10, 'm')
title('ECDF Varying Beamwidth (deg), 10dB Rx SNR')
xlabel('x')
ylabel('f(x)')
legend('52.59', '4.23', '2.21', '1.49', '1.13', '0.91', '0.76',...
'0.65', '0.57', '0.51')
grid
set(gcf,'color','white')
hold off
```

LIST OF REFERENCES

Berger, D. (2019). 38th Commandant's Planning Guidance CPG. USMC. https://www.marines.mil/News/Publications/MCPEL/Electronic-Library-Display/Article/1907265/38th-commandants-planning-guidance-cpg/

Chandler, J. (2014). DARPA's mobile hotspot program drives E-band performance benchmarks. *Microwave Journal, 57*(10), 22–22,24,26,28,30,32. Retrieved from http://libproxy.nps.edu/login?url=https://www-proquest-com.libproxy.nps.edu/trade-journals/darpas-mobile-hotspot-program-drives-e-band/docview/1614633291/se-2?accountid=12702

Dahlman, E., Parkvall, S., Sköld, J. (2018). What is 5G?. In, *5G NR: The Next Generation Wireless Access Technology* (pp. 3–4). Elsevier.

Garcia, A. E., Ozger, M., Baltaci, A., Hofmann, S., Gera, D., Nilson, M., Cavdar, C., & Schupke, D. (2019). Direct air to ground communications for flying vehicles: Measurement and scaling study for 5G. *2019 IEEE 2nd 5G World Forum*, 310–315. https://doi.org/10.1109/5GWF.2019.8911712

George, J. M. (2019, May). Spectrum warfare integration. *Marine Corps Gazette.* 59–62.

Giordani, M., Polese, M., Roy, A., Castor, D., & Zorzi, M. (2019). Standalone and non-standalone beam Management for 3GPP NR at mmWaves. *IEEE Communications Magazine*, *57*(4), 123–129. https://doi.org/10.1109/MCOM.2019.1800384

Greenberg, M. (2020). It's time to fix the command post: optimizing headquarters' mobility, survivability, and interoperability for the future fight. (2020, August 19). *Modern War Institute*. https://mwi.usma.edu/its-time-to-fix-the-command-post-optimizing-headquarters-mobility-survivability-and-interoperability-for-the-future-fight/?utm_source=rss&utm_medium=rss&utm_campaign=its-time-to-fix-the-command-post-optimizing-headquarters-mobility-survivability-and-interoperability-for-the-future-fight

Harvey, J. F., Steer, M. B., & Rappaport, T. S. (2019). Exploiting high millimeter wave bands for military communications, applications, and design. *IEEE Access*, 7, 52350–52359. https://doi.org/10.1109/ACCESS.2019.2911675

Heimann, K., Tiemann, J., Yolchyan, D., & Wietfeld, C. (2019). Experimental 5G mmWave beam tracking testbed for evaluation of vehicular communications. *2019 IEEE 2nd 5G World Forum (5GWF)*, 382–387. https://doi.org/10.1109/5GWF.2019.8911692

Hosseini, N., Jamal, H., Haque, J., Magesacher, T., & Matolak, D. W. (2019). UAV command and control, navigation and surveillance: a review of potential 5G and satellite systems. *2019 IEEE Aerospace Conference*, 1–10. https://doi.org/10.1109/AERO.2019.8741719

Krim, H., & Viberg, M. (1996). Two decades of array signal processing research: the parametric approach. *IEEE Signal Processing Magazine*, *13*(4), 67–94. https://doi.org/10.1109/79.526899

MathWorks. (n.d). *phased.Platform*. https://www.mathworks.com/help/phased/ref/phased.platform-system-object.html

MathWorks. (n.d.). *phased.RootMUSICEstimator.* https://www.mathworks.com/help/phased/ref/phased.rootmusicestimator-system-object.html

MathWorks. (n.d.). *phased.ULA.* https://www.mathworks.com/help/phased/ref/phased.ula-system-object.html

Medin, M., & Louie, G. (2019). *The 5G ecosystem: risks and opportunities for DOD*. Defense Innovation Board.

Nordum, A., Clark, K. (2017 January 27). *Everything you need to know about 5G*. IEEE Spectrum. https://spectrum.ieee.org/video/telecom/wireless/everything-you-need-to-know-about-5g

Stutzman, W. L., Thiele, G. A. (2013). *Antenna theory and design.* John Wiley &Sons.

Sun, X., Yang, W., Cai, Y., Ma, R., & Tao, L. (2019). physical layer security in millimeter wave SWIPT UAV-based relay networks. *IEEE Access*, 7, 35851–35862. https://doi.org/10.1109/ACCESS.2019.2904856

Tsirlis, C. S. (2020, April). Spectrum contested environments. *Marine Corps Gazette*.

Vondra, M., Dinc, E., Prytz, M., Frodigh, M., Schupke, D., Nilson, M., Hofmann, S., & Cavdar, C. (2017). Performance study on seamless DA2GC for aircraft passengers toward 5G. *IEEE Communications Magazine*, 55(11), 194–201. https://doi.org/10.1109/MCOM.2017.1700188

Wallace, H. B. (2014, October 30). *DARPA MMW system programs and how they drive technology needs* [Presentation]. DMRC Millimeter-Wave Technology Workshop. https://www.ece.ucdavis.edu/dmrc/files/2014/09/Bruce_wallace_darpa_web.pdf

INITIAL DISTRIBUTION LIST

1. Defense Technical Information Center
   Ft. Belvoir, Virginia

2. Dudley Knox Library
   Naval Postgraduate School
   Monterey, California